# A study of the formation of folding that extend to a 3D morphology in insects

Haruhiko Adachi

Laboratory of Pattern Formation
Graduate School of Frontier Biosciences, Osaka University

March 2022

# Abstract

Morphogenesis mechanisms are an important issue in the field of developmental biology. In the study of morphogenesis, much research has focused on embryogenesis, which is the process of drastic morphological change from a single cell. On the other hand, morphogenesis after embryonic development is not well understood. Metamorphosis is a characteristic example of drastic morphological changes that occur after embryogenesis. It is important issue to analyze the morphogenesis of metamorphosis in that the size scale is different from embryogenesis. In this study, I focused on the insect especially beetle horn and treehopper, morphogenesis through molting in the post-embryonic development.

Beetle horns are not present in the larvae, but suddenly appear when the beetle molts into a pupa. In a previous study, it was reported that beetle horns exist in a folded state in the head of the final instar larvae just before molting, and that simply physically expanding them would result in the final horn shape. On the other hand, there was no understanding of how the folding formation was controlled. Therefore, in this study, I first analyzed the formation of the horn primordia in the beetle. Analysis of the horn primordia of *dachsous* (*ds*) RNAi, which were known to get thicker and shorter horns, revealed that the macro shape of the horn primordia (especially the stalk portion of the mushroom morphology) changed significantly, while the micro furrows remained almost unchanged. Analysis of cell division showed that the anisotropy of cell division was abolished in *ds* RNAi. This suggests that macroscopic morphology and microscopic wrinkles are independently regulated, and that anisotropy of cell division is involved in macro shape. From the analysis of beetle of different body sizes, it was found that the depth of microscopic wrinkles and surface pattern (direction) did not change with size. Then, I searched for RNAi individuals in which these parameters were changed. As a result, I found that the notch gene and *cyclinE* gene play important roles in each. In addition, I found that in the control primordia, the frequency of cell division was higher in the areas where concentric folding patterns were expected to form than in other areas. In addition, in *notch* RNAi, the pattern of cell division was not disrupted, but the overall frequency of division was reduced, as seen in controls. Furthermore, in *cyclinE* RNAi, the frequency of cell division was reduced compared to controls only in areas where concentric folding patterns were expected to form.

These results indicate that the pattern (direction) and depth of folding of the horn primordia of the beetle are formed by independent mechanisms. It was also suggested that the regulation mechanism could be the control of the overall cell division frequency and the pattern of division frequency.

Next, in order to confirm the hierarchical developmental process observed in beetle horns, which also occurs in the morphogenesis of hemimetabolous insects, helmet structure of the treehoppers, which suddenly appears during molting into an adult, was focused on. Histological analysis using a combination of μCT, SEM, and paraffin sections revealed a continuous process of macro shape and micro furrow formation, suggesting the existence of a universality of morphogenesis process through folding and unfolding.

# Contents

# Chapter 1

# General introduction

Morphogenesis mechanisms are an important issue in the field of developmental biology. In the study of morphogenesis, much research has focused on embryogenesis, which is the process of drastic morphological change from a single cell. On the other hand, there is also a phenomenon that causes drastic morphological changes after embryogenesis, like known as metamorphosis. It would be important to analyze the morphogenesis of metamorphosis in that the size scale is different from embryogenesis. However, morphogenesis after embryonic development is not well understood except for a few model organs, partly due to its size, which makes it difficult to analyze.

In this study, I focused on morphogenesis through molting in insects, which induces drastic morphological changes after embryogenesis.

## 1.1 Differences between arthropod growth and vertebrate growth

In many animals, including vertebrates, their epidermis is composed of epithelial tissue consisting of epidermal cells and dermal cells. The development of those cells during the growth allows the body size to increase. On the other hand, in arthropods, including insects, there is a cuticular structure on the outside of a single epithelial cell sheet (Gullan and Cranston 2014, Hadley 1982). The cuticle is a hierarchical structure and is composed mainly of chitin, a polysaccharide linked to N-acetylglucosamine (Raabe et al. 2005), and is not a cell, so it cannot proliferate. In addition, cuticle is usually a rigid structure with limited elasticity, which prevents it from growing large during growth. Therefore, many arthropods employ an alternative strategy of molting, in which the old exoskeleton is replaced by a new one to allow for growth. The new exoskeleton forms inside the old exoskeleton, making it somewhat smaller at first. However, the newly formed cuticle has furrows, and these furrows are expanded during the molt, eventually allowing the body to grow larger (Chapman 1998). And with each successive molt, the animal grows larger, and its outline becomes

more complex. There is a phenomenon that causes drastic morphological changes after molting, called metamorphosis.

## 1.2 Insect model animal *Drosophila melanogaster* case

For example, in *Drosophila melanogaster,* an insect model organism, organs such as legs and wings are apparently absent in the larvae and pupae, but clearly present in the adults. *Drosophila* has long been used as a research model because of its ease of handling. In the process, *Drosophila* genetics and imaging techniques have been established (Hales et al. 2015). The adult organs of *Drosophila* exist as imaginal discs in the larval stage, differentiate and proliferate at the appropriate time, and have even been analyzed at the molecular level (Morata 2001). In the pupal stage, the mature imaginal disc is expanded through a step called eversion (Fristrom and Fristrom 1975, Aldaz, Escudero and Freeman 2010). Even after eversion, cell rearrangement and changes in cell shape occur until the adult wing is complete (Ray et al. 2018). Thus, the mechanism of metamorphosis is gradually being understood using the ease of handling of *Drosophila*.

However, in the case of *Drosophila* metamorphosis, the morphology formed by molting is simple structure, e.g., legs are rod-shaped, and wings are flat. In order to investigate the universality of the morphogenetic mechanism, it is necessary to examine other organs that undergo drastic deformation through molting. In this study, the formation of the horn structure of the beetle and the helmet structure of the treehopper, which acquire distinct complex 3D morphologies before and after molting were focused on and analyzed their formation mechanisms.

# Chapter 2

# Development of beetle horn

## 2.1 Introduction

Insect traits, such as the exaggerated horn of the beetles, develop under the larval cuticle, but the beetle horn appears in a relatively short period of time (within two hours) at pupation (Matsuda et al. 2017). The horn primordia consist of a furrowed epithelial cell sheet with cuticle located under the larval head cuticle. At molting, the primordia is extended to form its final 3D shape as blowing up furrows like a balloon. This transformation from furrowed primordia to final horn does not required any living cell activities (Matsuda et al. 2017). This indicates that the information for the final 3D structure of the beetle horn is patterned within the primordia by this time. On the other hand, there was no understanding of how the folding formation was controlled. Therefore, in this chapter, I analyzed the formation of the horn primordia in the beetle which consist of the information of complex 3D horn morphology (Fig.2-1-1). Matsuda et al.,2017 showed the morphological changes along developmental stages of the horn primordial cross-section. (Fig. 2-1-2). From these results, it seemed that the formation of the primordia was a continuous process that involved the formation of the mushroom-like macro shape and the micro furrows on its surface. I first decided to establish an internal observation method using micro-CT in order to clearly grasp the three-dimensional morphology of the horn primordium. Since it was not possible to see the horn primordia clearly by micro-CT observation using the usual fixation method, I established an observation method combining freeze-drying and alkaline treatment. Since insect cuticle is mainly composed of chitin, its morphology remains even after a certain amount of alkaline treatment. On the other hand, since the tissue inside the cuticle is mainly composed of protein, it is dissolved by alkaline treatment (Porto, Melo and Almeida 2016). Observations using this technique also shows that the horn primordia are composed of a mushroom-like macro shape and micro furrows on its surface. Micro furrows are further comprised of both the depth and the pattern. (Fig. 2-1-3). The mushroom-like macro shape can be further broken down into several parts (each part is named "stalk" and "cap" after the mushroom (Carroll 1989)) (Fig. 2-1-4). What remains unknowns is the morphological, molecular

and cytological properties of the macro shape and micro furrows which are not well understood. In this study, I investigated the factors determining the property of macro shape and micro furrows in the developing beetle head horn primordia and linked them to the final 3D horn structure. I firstly focused on horn primordia of *dachsous* (*ds*) RNAi, which were known to have thicker and shorter horns (Gotoh et al. 2015, Hust et al. 2018). Second, I explored the other genetic and environmental factors that cause each parameter to be altered.

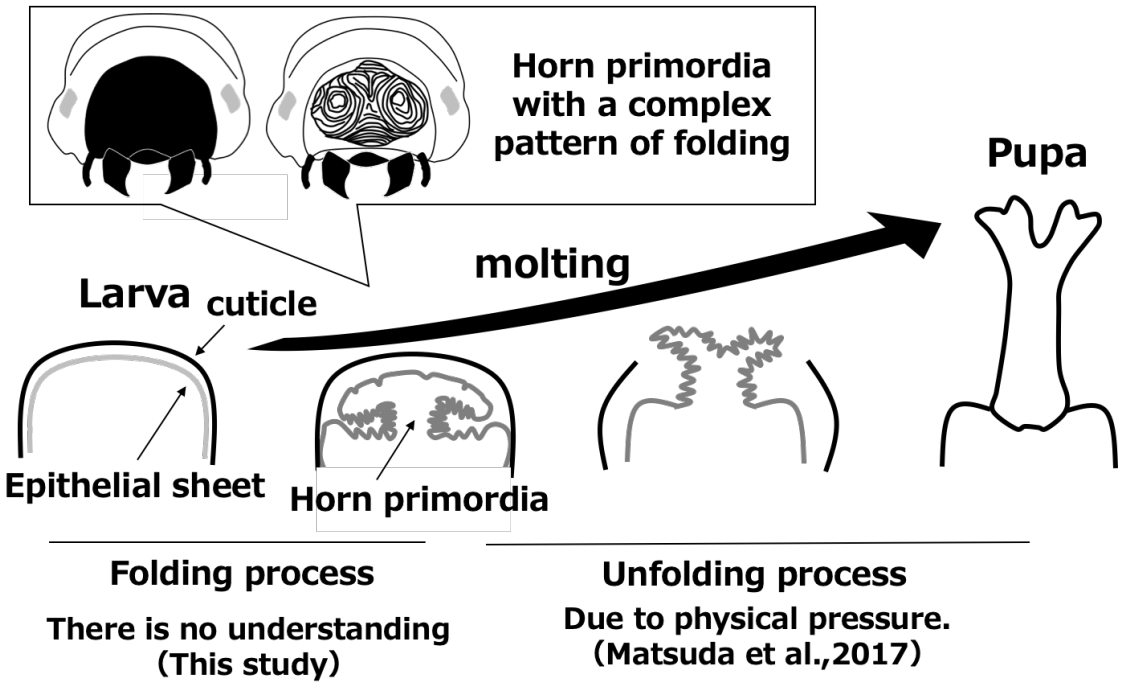


Fig. 2-1-1. Focus of this study; Formation of beetle horns by folding and unfolding of cell sheets

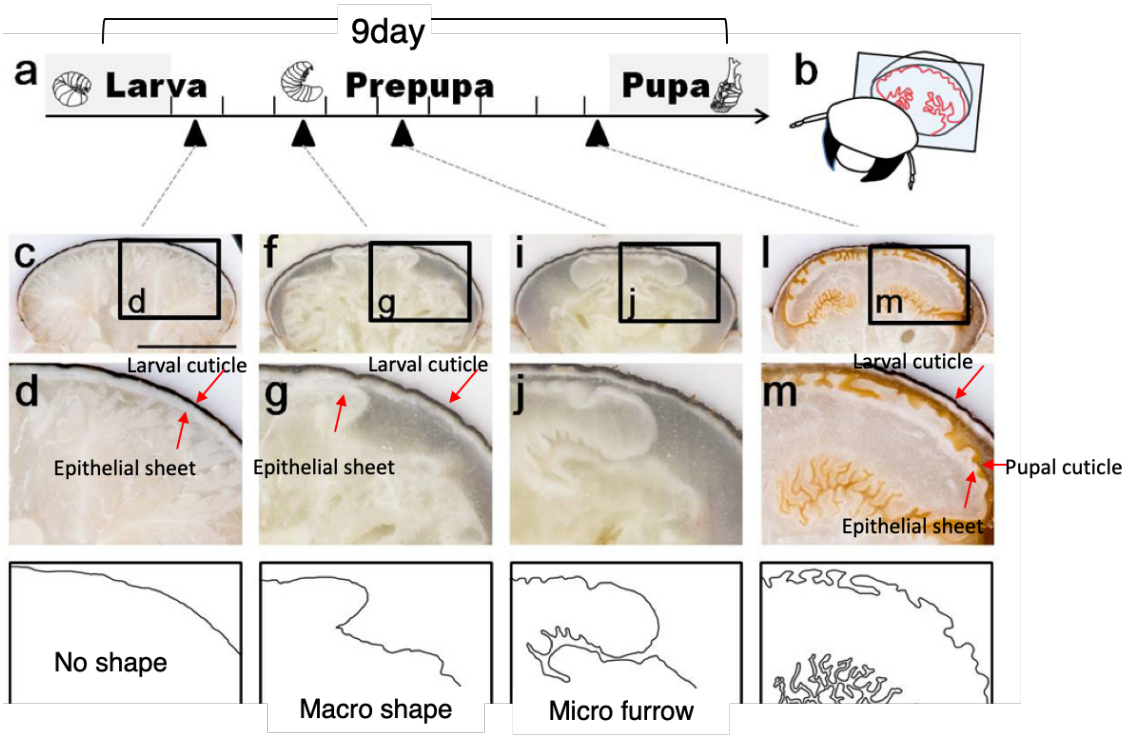


Figure modified from Matsuda et al.,2017.

Fig. 2-1-2. Developmental dynamics of the cross-section of horn primordia (Modified from Matsuda et al.,2017).

In the early stages of development, a single epithelial cell sheet is present along the larval cuticle (c,d), but as development progresses, the cell sheet first caves in, revealing the outline of a mushroom-like macroscopic morphology (f,g). As development progresses, microscopic wrinkles begin to form on the surface as the macroscopic form grows (i,J). Eventually, a pupal cuticle develops on the surface of the epithelial cell and is colored brown (l,m).

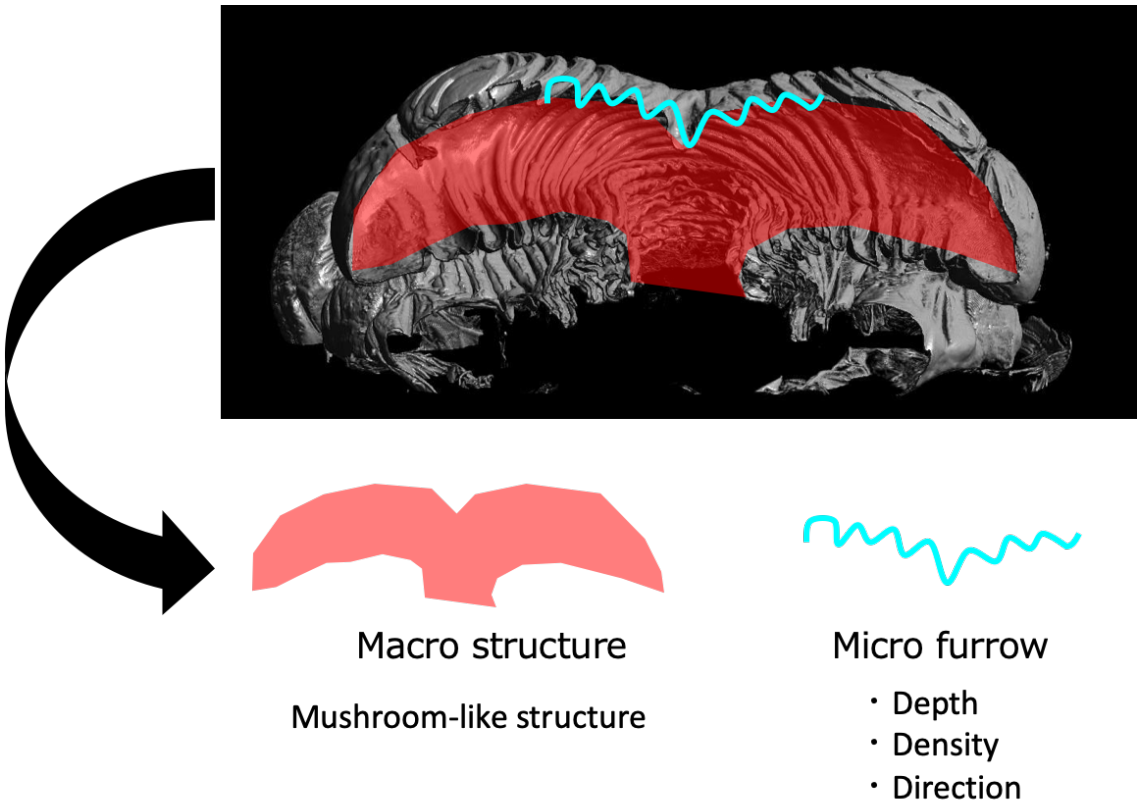


Figure 2-1-3. The morphology of the horn primordia

The horn primordia contain a mushroom-like macro structure and surface micro furrows. Micro furrows have depth, density and direction (2D furrow pattern).

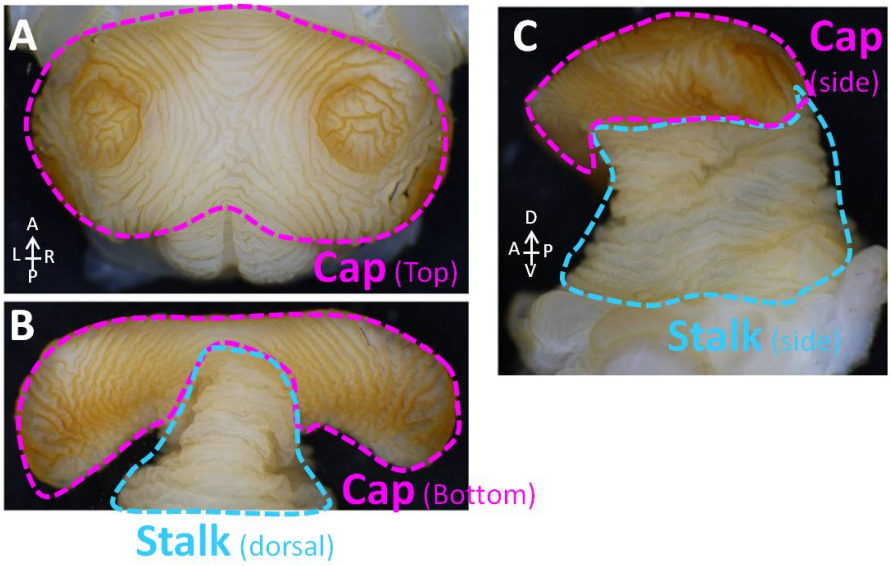


Fig. 2-1-4 Name of specific region in the horn primordia macro shape

Name of each region of horn primordia is according to Matsuda et al. 2017. Briefly, the horn primordia have a mushroom like morphology. A round-shaped area with two distinct central circles and two less obvious central circles was named the "Cap" area (indicated by the pink dashed line). This area will become branched structure at most distal position of pupal horn. The vertical column under the cap is named "Stalk" (indicated by the light blue dashed line). This area will become the long stem of the pupal horn. A) Dorsal view of primordia. Cap region with centric circles can be seen. B) Bottom of cap region. C) Side view of primordia.

## 2.2 Material and method

Insects

The beetle larvae were purchased and kept as bellow. Commercially purchased last instar (third instar) larvae of the Asian rhinoceros beetle *Trypoxylus dichotomus* were kept individually in 1 L or 800 mL plastic bottles filled with rotting wood flakes at 10–15 °C to suspend their development. Larvae were moved to 25 °C to restart their development before the experiments and/or observations. Bottles were checked daily in order to record the initial date of pupal chamber formation. Day 1 was defined as the first day when the pupal cell was clearly recognized. Most male prepupae pupated at Day 9, therefore I used Day 8 horn primordia with brownish color (a sign of sclerotization) as fully developed ones. Pupae and prepupae were weighed before each experiment. I used 7.28 to 18.05 g pupae and 8.95 to 21.30 g prepupae for analysis size-dependent parameters. For RNAi screening and RNAi-induced horn primordia phenotype analyses, I used a range of pupae from 13.66 to 23.35 g.

Dissection of horn primordia

Prepupae were anesthetized on ice before dissection. Amputated prepupal heads were fixed with 4% Formalin for overnight. Dissections were performed under a binocular microscope (SZ61-TRC, Olympus, Tokyo, Japan) and pictures were captured by a digital camera (EOS DIGITAL, Canon, Tokyo, Japan). Cross areas of the primordia stalk region in wildtype and dsRNAi animals were measured by using Fiji (Image J) (Schindelin et al., 2012). Sectioned images were taken by block-face imaging (Matsuda et al. 2017, Tajika et al. 2017), amputated prepupal heads were mounted in OCT compound (Sakura Finetek, Tokyo, Japan) without any chemical fixations.

Analysis of pupal horn morphology

Pupal horns were photographed using a digital camera (MZ16FA, Leica, Germany). The inflection point was used as a landmark and the length was measured using Fiji (Image J). For the length of the side groove and cap side stalk, both sides (right and left) were measured and averaged.

Degradation of inner structure of the primordia

The primordia have an inner structure containing muscle, tracheae and body fluid in addition to cuticle. To observe cuticular structure clearly, I degraded the inner tissue by incubating overnight with 10% KOH solution at 60 ℃ followed by washing with DDW and dehydration with ethanol. The dehydrated sample was soaked with t-butanol and freeze-dried. The sample was used for μCT observation and expansion experiments to observe the final horn shape of notch RNAi.

μCT scanning

Prepupae were anesthetized on ice and frozen using liquid nitrogen. The frozen samples were truncated by sawtooth. The truncated heads were dried using a freeze-drying system (FZ-2.5, Asahi Life Science, Japan) over 7 hours. Then the dried samples were scanned using a micro-CT scanner (Skyscan1172, Bruker, USA) following the manufacture's instruction. The X-ray source ranged from 40 kV, and the datasets were acquired at a resolution of 9 μm / pixel. The stacks of transverse sections were reconstructed from primary shadow images using SkyScan software NRecon. From these image stacks, 3D volume-rendered images were constructed using SkyScan software CT Vox.

Analysis of the horn primordia morphology

The equal-section images were obtained using landmarks such as the points changing furrow direction and inflection points of macro structures (Fig. 2-2-1) using SkyScan software Data Viewer. Firstly, the length of the cap region of the mushroom-like macro structure of the section images was measured. Then the density of furrows was calculated from the number of furrows per the length of measured region. The average depth of individual furrows was calculated from the depth of all furrows in the measured region. All data were measured using Fiji (Image J). Also, in the bottom region of the mushroom-like macro structure, the same analysis was conducted.

Nuclei staining

Prepupae were anesthetized on ice before dissection. Amputated prepupal heads were fixed with 4% PFA for 2 days at 4 ℃. Dissections were performed under a binocular microscope (SZ61-TRC, Olympus, Tokyo, Japan) Dissected PFA-fixed primordia were further divided into small pieces under a binocular microscope. During this process, the original position within each primordia

fragment was recorded. Fragment tissues were washed with PBS(-) three times and incubated at room temperature for 60 minutes with Hoechst 33342 (1:1000, Invitrogen) in 1% BSA solution, then washed with PBS(-) three times, before tissues were mounted on a glass slide and covered with a cover glass. Fluorescent images were observed and recorded with a confocal laser scanning microscope (LSM-780; Carl Zeiss, Jena, Germany).

Analysis of cell division

Dissected tissue from developing horn primordia at prepupal Day 4 was stained by Hoechst because the timing is just before formation of many micro furrows (Fig. 2-2-2) and cell division occurs frequently during this time. All of the dividing cells and the angle of each division of the primordia were measured using Fiji (Image J) (Schindelin et al. 2012). In cap region, the five regions (center, upper, lower, left, and right) were determined based on a pair of crescent-shape furrows (Fig. 2-2-2). In stalk region, angle of cell division against micro furrow was measured using Fiji (Image J) (Schindelin et al., 2012). Three different areas per one tissue were analyzed.

RNA extraction and RT-PCR for dsRNA synthesis

Horn primordia tissue was homogenized in 200-500 μL of Isogen (Nippon Gene), and 1/5 of the volume of Isogen was added to Chloroform, vortexed, and allowed to stand at room temperature for 2 minutes. Then, centrifuge at 4°C for 15 minutes (15,000 rpm). Add an equal volume of Chloroform to the supernatant (3/5 of Isogen), mix by inverting, and centrifuge at 4°C for 5 minutes (15,000 rpm). To the supernatant (1/2 volume of Isogen), an equal volume of Isopropanol was added, stirred, and allowed to stand at room temperature for 10 minutes. The mixture was then centrifuged at 4°C for 30 minutes. RNA samples were prepared by washing the precipitates with 70% ethanol and dissolving them in distilled water. RT reactions were performed using TOYOBO's ReverTra Ace kit. The concentration of RNA samples was measured using BioPhotometer. 5 μg of RNA sample in 6 μL of total was added to RNAase free water after heating/quenching at 65°C for 5 min. The RNA sample was heated/quenched at 65°C for 5 min, adjusted with RNAase free water to contain 1 μg of RNA sample in 6 μL total, and incubated with 2 μL of RT Master Mix II at 37°C for 15 min, 50°C for 5 min, and 98°C for 5 min, and then 90 μL of DDW was added to make a cDNA sample. cDNA sample obtained by RT reaction was diluted 10-fold, and PCR was performed using primers. (94°C

5m, [94°C 10s, 55°C 20s, 68°C 1m] × 35 cycles, 68°C 10m 25°C ∞) PCR products were visualized with ethidium bromide after agarose gel electrophoresis and the amplified sequence was cut out from the gel and purified by a gel extraction kit (QIAGEN, Germany). dsRNA was synthesized using the MEGAscript RNA kit (Ambion, Austin, TX, USA) using the purified partial sequence of the Trypoxylus gene as a template. The T7 promoter sequence (TAATACGACTCACTATAGGG) was added to the primer sequences, and the respective sequences are shown in Table 2-2-1.

Gene knockdown via RNAi

I searched the ortholog mRNA sequence from the RNAseq database of T. dichotomus (PRJDB6456) using D. melanogaster sequences as a query via the tblastn program (Morita et al. 2019). Gene knockdown was performed via RNA interference (RNAi). Briefly, the partial sequence of Trypoxylus genes were amplified by a specific primer with an attached T7 sequence. The amplified sequence was cut out from the gel and purified by a gel extraction kit (QIAGEN, Germany). dsRNA was synthesized using the MEGAscript RNA kit (Ambion, Austin, TX, USA) using the purified partial sequence of the Trypoxylus gene as a template. Synthesis, purification, and storage of dsRNA were performed according to manufactures protocol. 5 μg of dsRNA was injected into late 3rd instar larvae using a 30 G needle syringe (BD, Japan).

Statistical analysis

Most of single comparisons statistic test was performed using Student's t test t by Microsoft Excel. The morphological parameters, the number and the angle of cell division in Ctrl, N RNAi, CycE RNAi were conducted in one-way analysis of variance (ANOVA test) followed by the Dunnet test using R console to compare the difference to controls. In this comparison, the number and angle of cell division in each region of N RNAi or CycE RNAi primordia were compared to the corresponding region of negative control primordia.

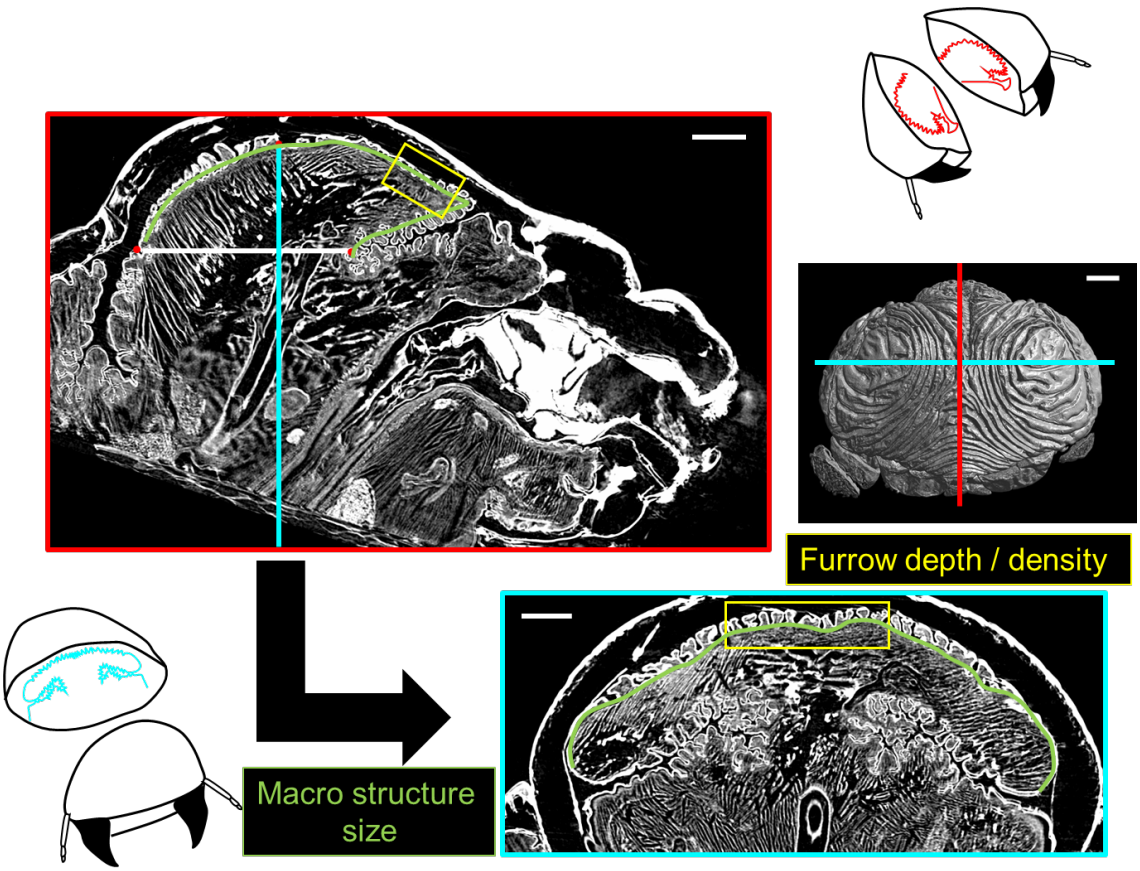


Figure 2-2-1. The area to analyze the morphological parameters

The equal-section images were obtained using landmarks such as the points of changing furrow direction and the inflection point of the macro structure of the primordia. Length of green line was measured as macro structure size. Furrow density and the depth were analyzed in yellow region by measuring depth of each furrow and counting number of furrows. Scale bar indicates 1 mm.

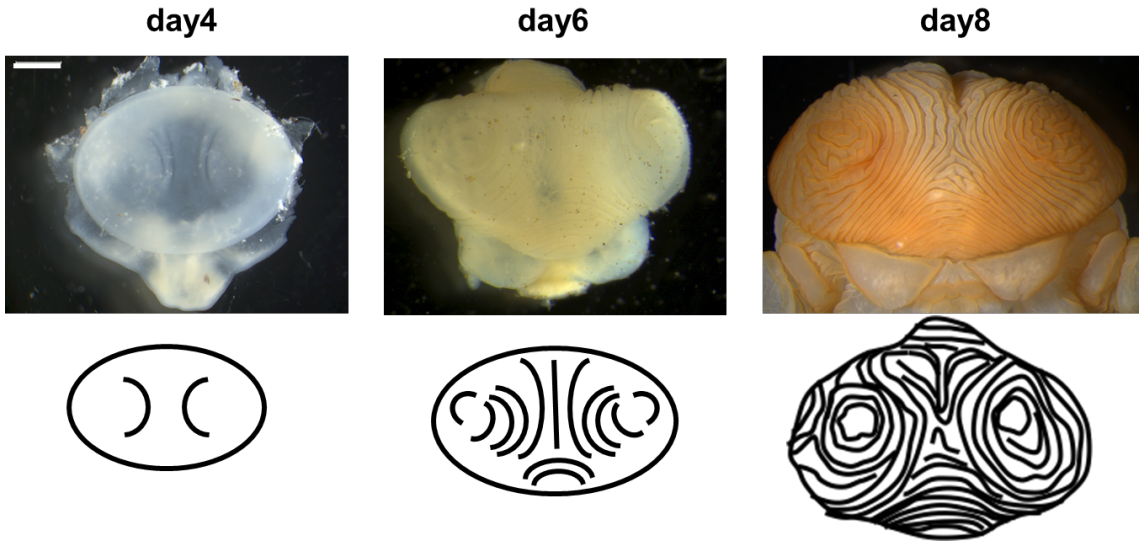


Figure 2-2-2. Chronological observation of the primordial furrow formation

A pair of crescent-shape furrows formed in the early stage (day4). Samples collected on day 4 were used for analysis of cell division. And the analysis in cap region, I used these furrows as a landmark to investigate cell division patterns across areas. Scale bar indicates 1 mm

Table 2-2-1: List of primer used for gene amplification as dsRNA synthesis temperate

| Gene name (accession number) | Forward sequence | Reverse sequence |
|---|---|---|
| *N* (IADJ01079691.1) | ACCGTTCAAACAAGGACTGG | CGTATCGCGAACTCTTGTGA |
| *CycE* (IADJ01090595.1) | CGTCGTAGAGAAATGCTGTAGC | GATCGGAGAAGGCGTCGACCTTTCGCG |
| *mud* (IADJ01075087.1) | TTGCCGGTCTTAATGTCCTC | GCCACTTTGCCGAGATGTAT |
| *ds* (IADJ01089570.1) | GTCAGGGAACTCGAGGTATCCGAAGG | CAGATCTAAATCCTTAGCCGGATGC |
| *Optix* ( IADJ01054575.1) | ACGAAAAGCTCTCACGGAAA | ACTCGCTAATTGGGCTGCTA |
| *rx* (IADJ01019649.1) | AGTGAAACCGTTGAGGATGG | GAACTCTGACTTCGGGCAAG |
| egfp(control) | CCTGAAGTTCATCTGCACCA | TGCTCAGGTAGTGGTTGTCG |

## 2.3 Result and discussion

The Dachsous genes contribute to the regulation of macro shape in the horn primordia, especially in the stalk region.

In *Drosophila*, Ds is likely to act as a ligand of Fat (Ft), which regulates planar cell polarity (PCP) and cell proliferation via the Fat-Hippo pathway (Reddy and Irvine 2008, Irvine and Harvey 2015). In the horn of the beetle (Trypoxylus dichotomus), it has been reported that knockdown of the ds gene during primordial development of the horn results in a shorter and thicker adult horn (Gotoh et al. 2015, Hust et al. 2018). In the case of pupae, the change in the shape of the horns were also observed (Fig.2-3-1A, B). In order to determine which parameters of the horn primordium are responsible for this change in horn shape, I first observed horn primordia just before molting by dissection (Fig.2-3-1 C-F). As a result, there was no drastic change in the furrows pattern on the surface of the horn primordia, but there was a significant change in the stalk region of the macro shape (Fig.2-3-1 C-G). For more detailed observation, the section of the frozen tissue was cut out using a technique established in previous study (Fig.2-3-1 H) (Matsuda et al. 2017, Tajika et al. 2017). Even in the cross section, there was no drastic change in the depth of furrows on the surface or in the interval, while the stalk region of the mushroom like macro shape became thicker (Fig.2-3-1 I, J). The observation of the horn primordia in the early stage of development showed that the morphological abnormalities caused by *ds* RNAi started to appear already after 4 days of pupal chamber preparation (Fig.2-3-1 K, L).

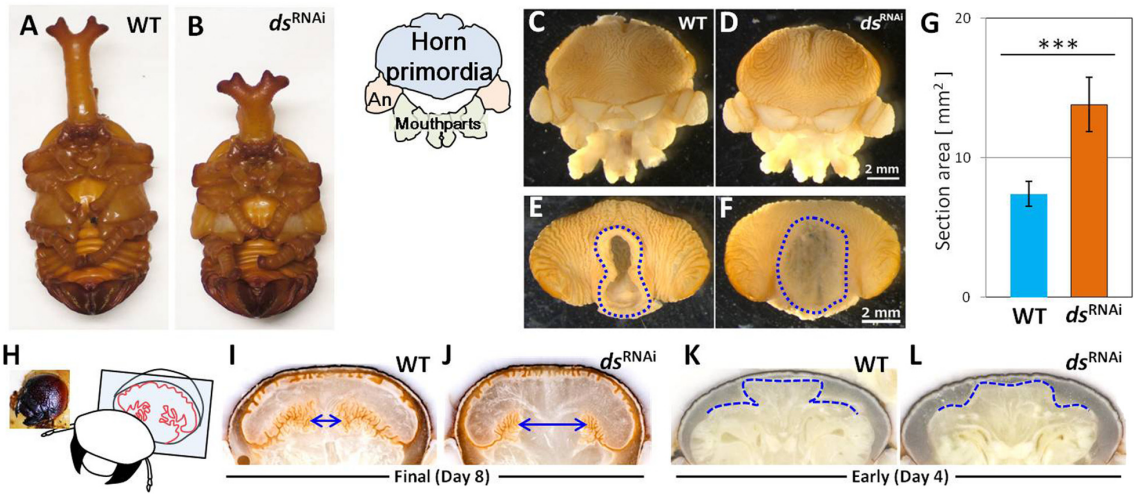


Fig. 2-3-1 Phenotypes of *ds* knocked down beetles

a, b) Pupa of wildtype and *ds* RNAi beetle. Horn morphology became thick and short in dsRNAi pupae. C, D) Dorsal view of fully developed horn primordia of wildtype and dsRNAi beetle, respectively. e, f) Ventral view of fully developed horn primordia of wildtype and dsRNAi beetle, respectively. Cross sectional areas of horn primordia stalk (future horn column) are indicated as dashed line. g) Cross sectional area of fully developed primordia stalks was significantly larger in dsRNAi beetles than in wildtype beetles ($P < 0.001$, student t-test). h) Schematic diagram indicating position and shape of sectioned horn primordia, shown in i, j, k and l, inside the prepupal head capsule. i, j) Frontal section of fully developed horn primordia of wildtype and dsRNAi beetle, respectively. Global shapes of primordia are mushroom-like, but stalks became thicker in dsRNAi beetles. Widths of the stalk were indicated by two-way arrows. k, l) Frontal section of early developing horn primordia of wildtype (k) and dsRNAi beetle (l). Morphological difference can be recognized from early prepupae. Blue dashed lines indicate shape of developing primordia. Note that the width of the stalk is already different.

The Dachsous gene contribute to the control of direction of mitosis

Next, I examined the cytological underpinnings of dsRNAi-induced changes in horn primordia shape. Given that *ds* is involved in establishing planar cell polarity (PCP) (Irvine and Harvey 2015, Segalen and Bellaïche 2009), the direction of cell division is a one of the candidate mechanisms for the difference in growth direction. Therefore, I measured the angle of cell divisions in the stalk region during the development of the horn primordia. In the stalk region, there was a clear direction of growth, with several furrows forming perpendicular to the growth direction (Fig.2-3-2). When epithelial cell sheets of the horn primordia stained with Hoechst were observed by confocal laser microscopy, many pairs of crescent-shaped nuclei were observed on the apical side of the sheets. In epithelial cells, the movement of the nucleus to the apical side, called elevator movement, occurs during cell division (Meyer, Ikmi and Gibson 2011, Woods and Bryant 1993), and this characteristic nucleus was stained by phosphorylated histone antibodies (Fig.2-3-2), suggesting that this nucleus is in the mitotic M phase (Callaini et al. 1994).

Hence, the nucleus angle of each division to the groove was measured at the stalk of the developing horn primordium. As a result, in the WT primordium, anisotropic cell division was observed (Fig 2-3-3A). That is, there were significantly more cells that divided along the direction of stalk growth and fewer cells that divided vertically against the direction of growth (Fig 2-3-3B). On the other hand, such anisotropy of cell division was disturbed in the *ds* RNAi (Fig 2-3-3B). These results suggest that the short and thick horn phenotype induced by *ds* RNAi is caused by the loss of cell division anisotropy and the change in the macro shape of the primordia (thick stalk) during its growth phase. Such anisotropic cell division is also known to be an important regulator of wing plate formation via PCP-regulated genes such as ds and ft in Drosophila (Baena-López, Baonza and García-Bellido 2005, Segalen and Bellaïche 2009, Mao et al. 2011). Thus, anisotropic cell division and its molecular regulators in organogenesis are likely to be conserved in different insect species (beetles and flies) and in different organs (horns and wings).

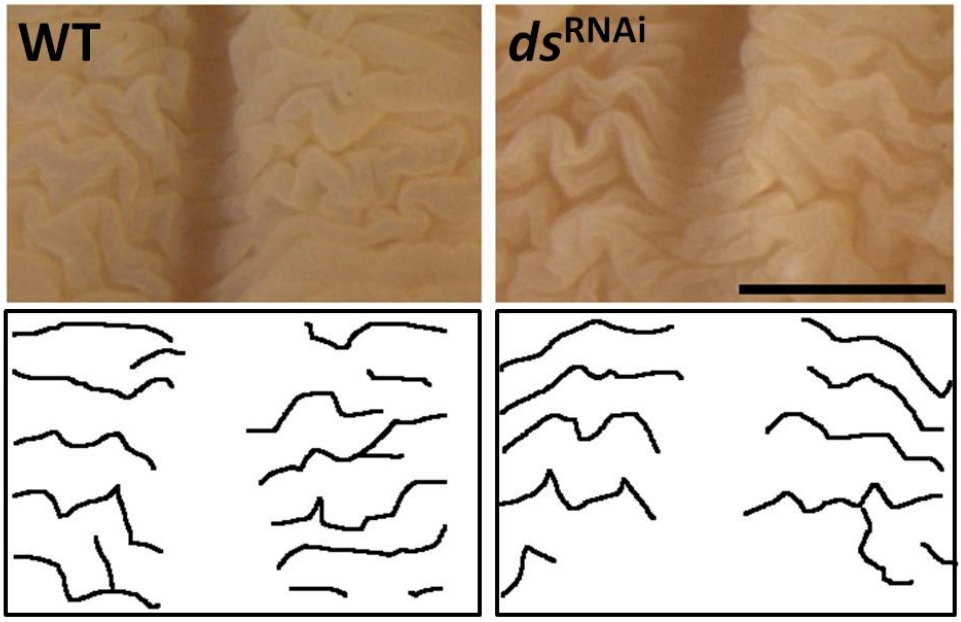


Fig. 2-3-2 Dorsal view of stalk area of fully developed horn primordia

Note that zigzag vertical furrows can be clearly recognized both in wildtype and dsRNAi beetles.Scale bar indicates 1 mm.

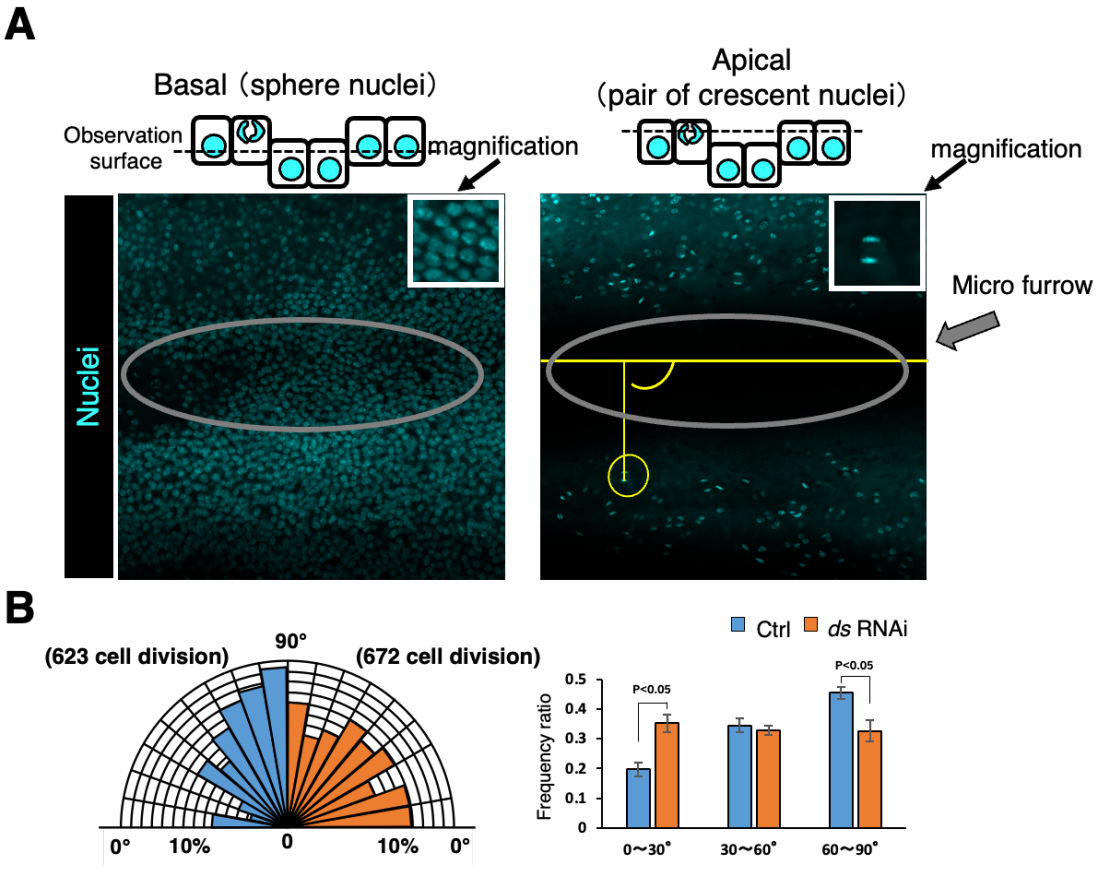


Fig. 2-3-3 Analysis of cell division of stalk region in WT and *ds* RNAi

a ) Method for analysis of the cell division angle. In epithelial sheets, dividing nuclei move to the apical side of cells when dividing known as elevator movement (Woods and Bryant 1993, Meyer et al. 2011). So, we can easily recognize most of cell division by observing the apical side of the epithelial sheet. Dividing nuclei can be recognized from their paired crescent shape (indicated as yellow round circle in right panel), so that the dividing angle against developing furrow can be calculated (yellow lines). There are few dividing nuclei in the basal side of the epithelial sheet (left panel). b) Analyses of cell division in developing horn tissue of wildtype and ds knockdown beetles Ratio of cell division direction in wildtype and dsRNAi beetles, respectively. (n =5 respectively).

The depth of the furrow and 2D furrow pattern is independent of body size

Adult beetle horns are also known to differ in length depending on body size, mainly due to growth conditions (Emlen, Corley Lavine and Ewen-Campen 2007, Emlen and Nijhout 1999, Johns et al. 2014, Warren et al. 2014, Emlen et al. 2012). Also in pupa, the size of the four-pronged tip region of the horn covaried with body size (Fig. 2-3-4). It has recently been shown that this four-pronged structure originates from the cap region of the horn primordium (Matsuda et al. 2021). Therefore, it was decided to focus on the cap region of the horn primordia for the next analysis. I investigated how the macro structure and micro furrows of the horn primordia contributed to variation in the size of the tip region and whether these parameters fluctuated simultaneously or independently. I analyzed the depth and density of furrows and mushroom-like macro structure size in different sized primordia because these factors can change the horn size (Fig. 2-3-5). I found that the depth of furrows was constant regardless of the body size (Fig. 2-3-6). The density of furrows was negatively correlated with body size, but its correlation coefficient was moderate (Fig. 2-3-6) or did not correlate in some areas (Fig 2-3-7,8). On the other hand, the macro structure size of the primordium was strongly correlated with body size (Fig. 2-3-6,7). This tendency (constant furrow depth, weak or no correlation of furrow density and strong positive correlation of macro structure) was also observed other regions of the horn primordium (Fig. 2-3-7,8). I also observed primordial surface 2D furrow patterns among different body sized animals. Specifically, I compared the surface furrow pattern (a pair of concentric-like furrows pattern) in both small and large larval primordia (Fig. 2-3-6 b). These data suggested that size-dependent morphological change in horns is primarily controlled by changing the size of the macro structure, rather than the depth of the primordium furrows.

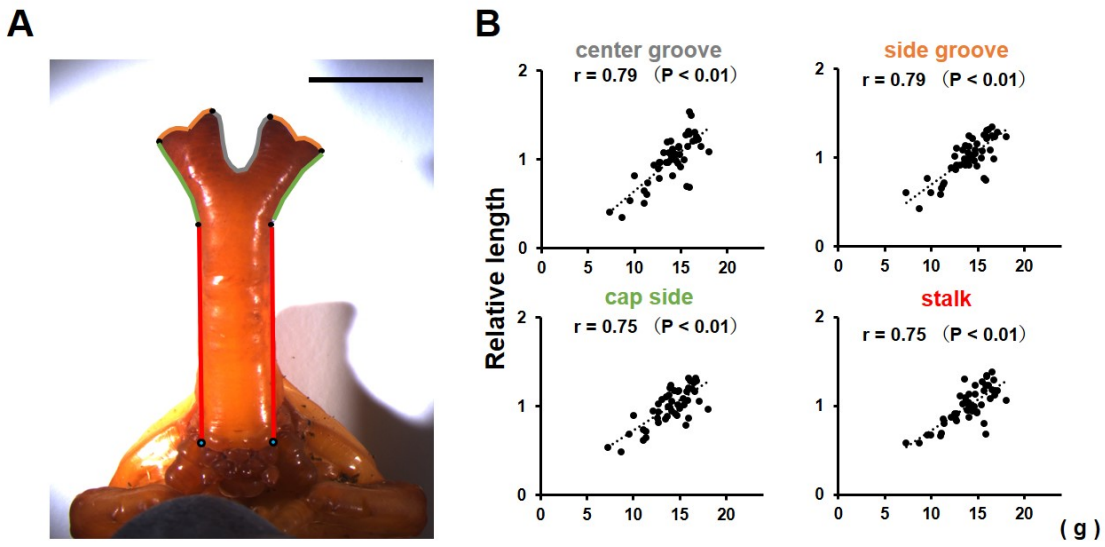


Figure 2-3-4. Relationship between body size and the morphology of the pupa

(a) Pupal horn with individual parts outlined. Landmarks were determined by inflection points. Scale bar indicates 10 mm. (b) Relationship between body size and the length of each part of the horn. Measured lengths of each horn part were strongly correlated with body size, and the scaling relationship (the slope) to body size are nearly identical (n = 48).

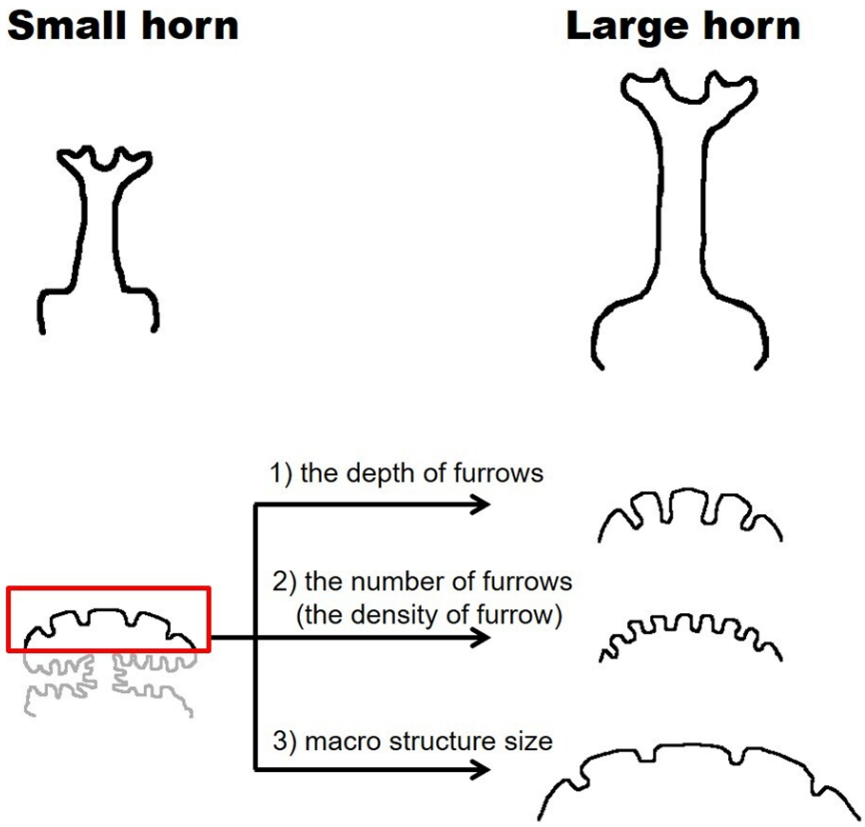


Figure 2-3-5. Three ways to increase the size of horn via changing morphological parameters of the primordia

There are three ways to increase the size of horn via changing morphological parameters of the primordia. First is increasing macro structure size. Second is increasing the number of furrows (in other words, increasing the density of the furrows). Third is increasing the depth of the furrows.

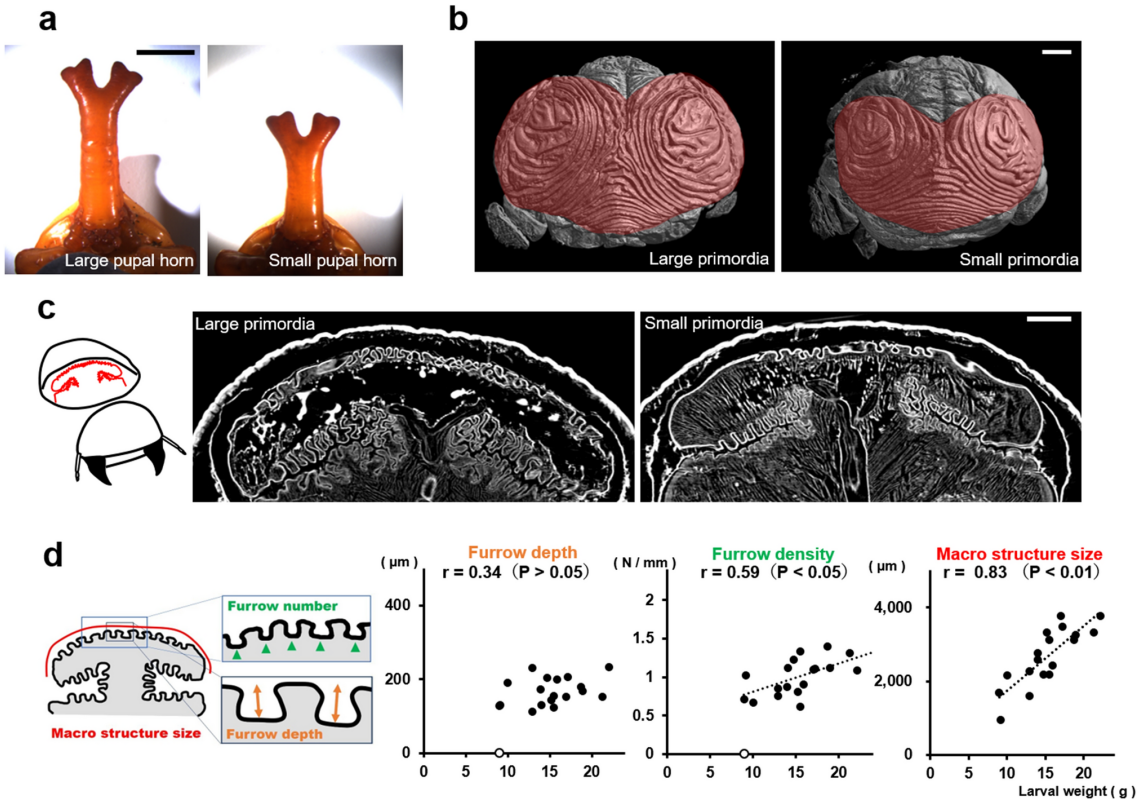


Figure 2-3-6. Relationship between body size and the morphology of the primordia at cap area.

(a) The horns of pupae with different body sizes (left: 18 g, right: 14 g). The larger beetle has the longer horn. (b) The primordia of the horn from different body sizes (left: 18 g, right: 14 g). Both of the primordia have similar 2D furrow patterns (concentric furrow patterns and stripe furrows between them), while the overall sizes of primordia are different. The cap (top) regions of the primordia are indicated in red. The images were acquired by μCT scanning. (c) Virtual frontal section images of horn primordia via μCT scanning. The mushroom-like macro structure can be recognized regardless of body size. (d) Relationship between body size and the macro structure size, the density of the furrows, and the depth of the furrows. For macro structure size the correlation coefficient was 0.83 ($p < 0.01$), for furrow density the correlation coefficient was 0.59 ($p < 0.05$), and for furrow depth, the correlation coefficient was not significant. In the smallest beetle (white plot: 8.95 g), obvious furrows could not be detected so it was excluded from the analysis ($n = 19$). Scale bar is 10 mm for (a), 1 mm for (b) and (c).

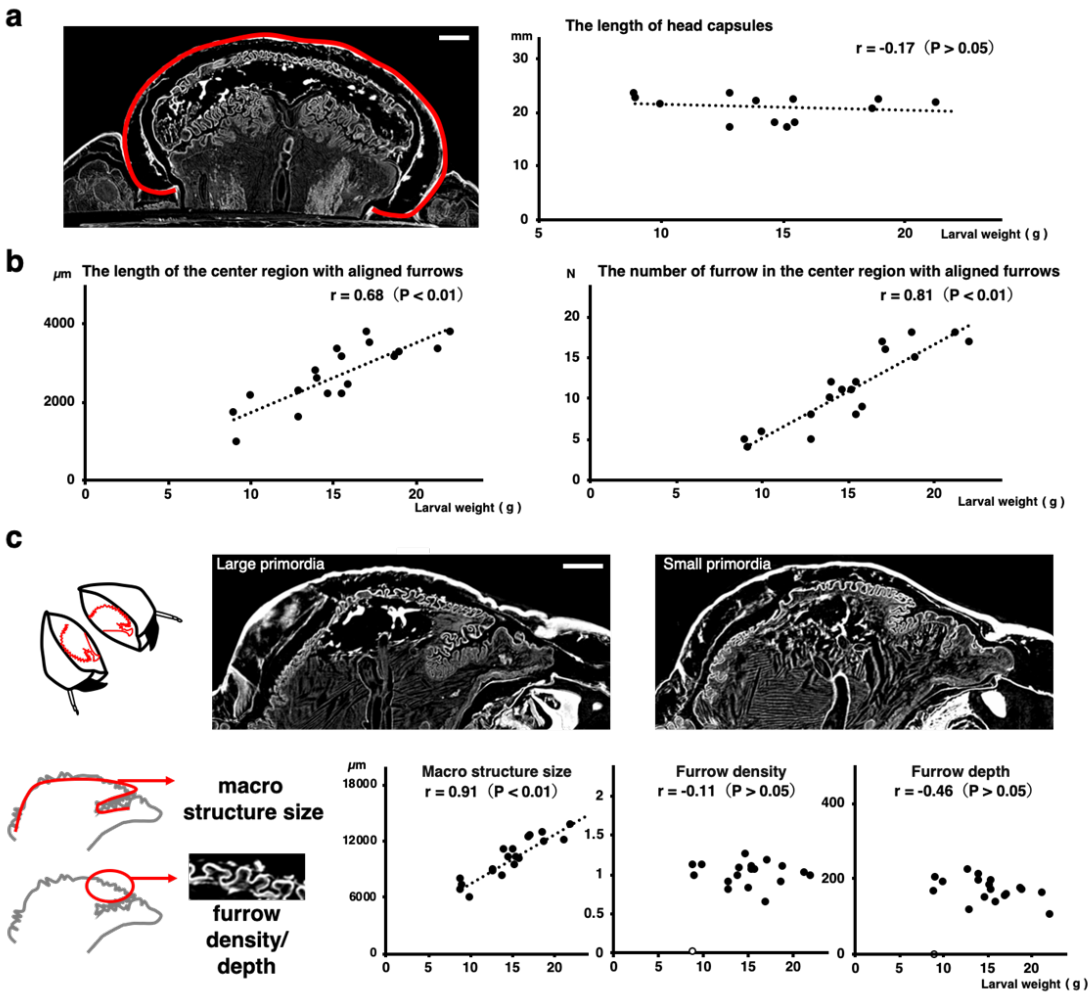


Figure 2-3-7. Relationship between body size and the morphology of the head cupsules and primordia (sagittal section)

(a) Relationship between body size and the size of the head cupsules. The correlation coefficients were not significant. (n = 13). Scale bar indicates 1 mm. (b) Relationship between body size and the primordial morphological parameters (the macro structure size, the density of the furrows, the depth of the furrows) in the sagittal section. For macro structure size, the correlation coefficient was 0.91 ($p < 0.01$), for furrow density and depth, the correlation coefficients were not significant. In the smallest beetle (white marker: 8.95 g), obvious furrows could not be detected, so it was excluded from the analysis (n = 19). Scale bar indicates 1 mm. (c) Relationship between body size and the primordial morphological parameters (the macro structure size, the density of the furrows, the depth of the furrows) in the sagittal section. For macro structure size, the correlation coefficient was 0.91

($p < 0.01$), for furrow density and depth, the correlation coefficients were not significant. In the smallest beetle (white marker: 8.95 g), obvious furrows could not be detected, so it was excluded from the analysis (n = 19). Scale bar indicates 1 mm.

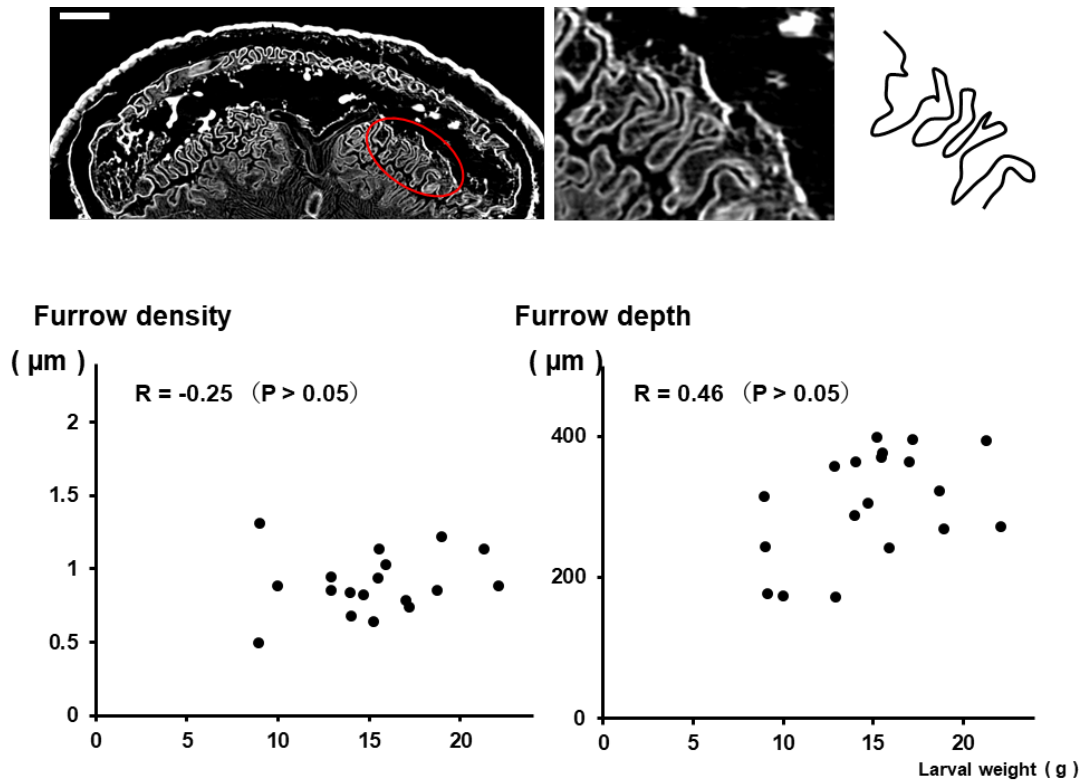


Figure 2-3-8. Relationship between body size and the morphology of the primordia (cap bottom region)

Relationship between body size and primordia parameters (the macro structure size, the density of the furrows and the depth of the furrows) in the cap bottom region. For furrow density and depth, the correlation coefficients were not significant (n = 19). Scale bar indicates 1 mm.

The Notch and cyclinE genes contribute to the control of furrow depth and 2D furrow pattern, respectively

The observations suggested that the depth and 2D patterns of the furrows are strictly regulated independently of body size. Hence, I next searched for the gene(s) involved in controlling furrow depth and 2D pattern. As mentioned above, methodology for use of RNAi is well established for beetles (Tomoyasu and Denell 2004, Angelini, Smith and Jockusch 2012), and horn shape can be changed by specific gene knockdown (Emlen et al. 2012, Ohde et al. 2018, Ito et al. 2013). I analyzed six candidate genes (Notch < *N* > , CyclinE < *CycE* > , mushroom body defect < *mud* > , Optix < *Optix* > , Retinal Homeobox < *rx* >), each already known to affect insect appendages and horn shape (Ohde et al. 2018, Wang et al. 2017, Crabtree et al. 2020), using RNAi to see how they affected the furrows on the horn primordia. Although I found several differences in primordium development in RNAi animals, I focused especially on *N* RNAi and *CycE* RNAi because these two changed the depth and 2D pattern of furrows (Fig. 2-3-9 a) more drastically than did the other candidate genes. *N* RNAi significantly decreased the depth of furrows relative to controls (*egfp* dsRNA injection) in almost all measured regions of the primordia (Fig. 2-3-9 b,c, 2-3-10), except for a pair of specific furrows (Fig. 2-3-9 b red arrowhead). In addition to decreasing furrow depth, macro structure size and the furrow density were increased in *N* RNAi beetles (Fig. 2-3-9 c, 2-3-10). I then manually extended the primordia to investigate the influence of changes in furrow depth on the final horn shape, because none of the *N* RNAi larvae survived until pupation. I found that in these manually extended horns the center groove and side groove were missing, and the shape of the horn tips were like the centroclinal primordial shape (Fig. 2-3-9 d). On the other hand, *CycE* RNAi changed the 2D furrow pattern (from concentric-like to zigzag-like) (Fig. 2-3-9 a, 2-3-11) and the resulting pupal horn shape (the center groove became shallower) (Fig. 2-3-9 e), while the macro structure size, and the density and depth of the furrows were not affected (Fig. 2-3-9 b,c, 2-3-10).

Recently, the contribution of Notch signaling to horn formation was also demonstrated in a dung beetle, *Onthophagus Taurus* (Crabtree et al. 2020). This study result is consistent with this, and I have found that Notch plays an important role in determining the final horn shape via regulating primordial furrow depth. In addition to the depth of the furrows, the density of the furrows and macro structure size of the primordia were also affected by *N* RNAi. Considering that the macro

structure size and the density of the furrow can vary depending on body size (Fig. 2-3-6 c,d), while the furrow depth did not, it is assumed that *N* RNAi has a direct effect on the depth of the furrow (i.e. the furrow density increasing in *N* RNAi likely to be a byproduct of the effect on furrow depth).

As for the relationship between the morphology of the primordium and pupal horn in *N* RNAi, it is suggested that the change of the depth of furrows causes the change of the final horn shape. Also, in *CycE* RNAi, it is presumed that the change of 2D furrow pattern causes the change of the pupal horn shape, because the different 2D furrow patterns can be extended to variable 3D structures. These results strongly indicate that both furrow depth and 2D furrow pattern are important parameters affecting final horn shape, but that they are regulated independently.

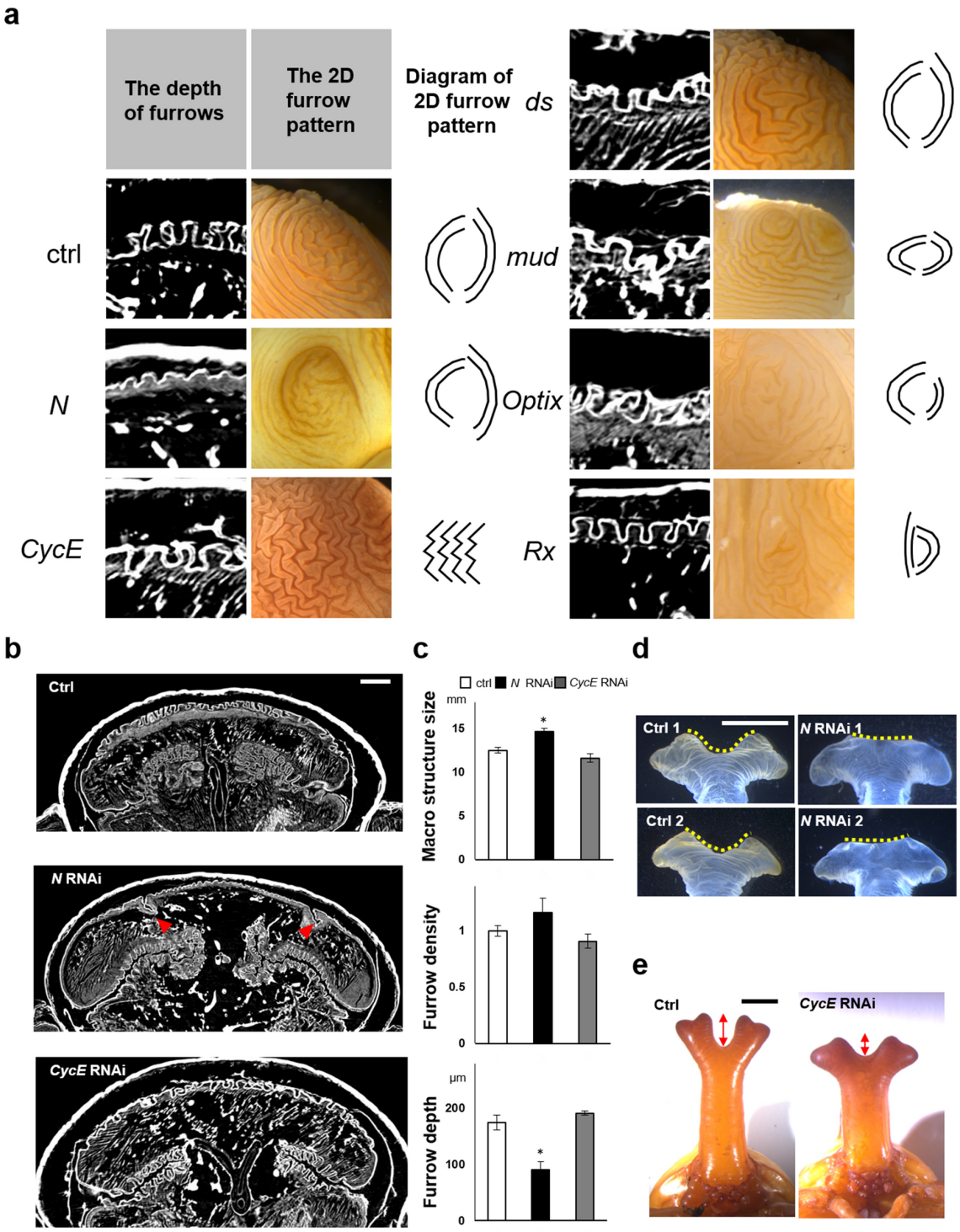


Figure 2-3-9. RNAi screening show that the Notch and CyclinE genes contribute to control of furrow depth and 2D furrow pattern, respectively

(a) Comparison of the depth and surface 2D pattern (concentric-like pattern) of the horn primordia between control and six different RNAi treatments. The 2D furrow patterns inside of the primordial top region were compared. *N* RNAi decreases the depth of the furrow and *CycE* RNAi disturbed the concentric-like 2D furrow pattern. (b) Comparison of the frontal section of the head just before pupation in control and *N* RNAi and *CycE* RNAi. The red arrowheads show the specific deeper furrows detected in *N* RNAi. (c) Quantitative data of the macro structure size and the density and the depth of the furrow (asterisk means $P < 0.05$) ($n = 7, 5, 6$ for negative control, *N* RNAi, *CycE* RNAi, respectively; however the furrows were too shallow to measure in one *N* RNAi so that $n = 4$ for furrow depth and density). (d) Pupal horn shape phenotypes between control and *N* RNAi. Two different individuals were shown in both of control and *N* RNAi. Marked differences of center groove depth were highlighted by yellow dashed line. (e) Comparison of the pupal horn shape between control and *CycE* RNAi. Marked differences of center groove depth were highlighted by red arrows. Scale bar indicates 1 mm for (b), 5 mm for (d) and (e).

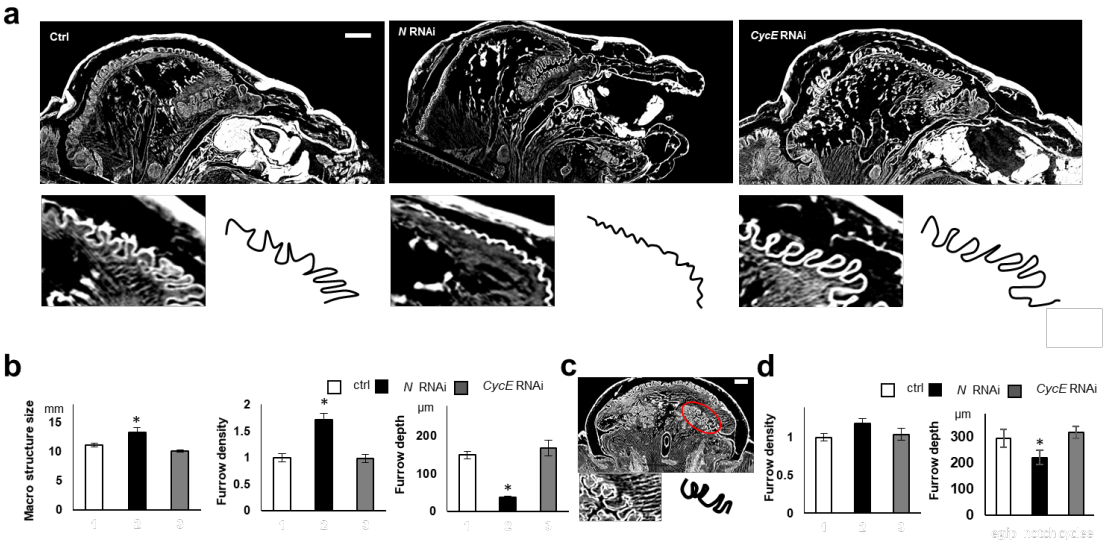


Figure 2-3-10. Morphological parameters of the primordia in *N* and *CycE* RNAi

(a) Comparison of sagittal section of the head just before pupation between control and *N* RNAi and *CycE* RNAi. (b) Quantitative data of macro structure size and furrow density and furrow depth from analysis ($n = 7, 5, 6$ for negative control, *N* RNAi, *CycE* RNAi, respectively). (c) Analysis point of the furrow in cap bottom region. (d) Quantitative data of furrow density and furrow depth in cap

bottom region (n = 7, 5, 6 for negative control, *N* RNAi, *CycE* RNAi). Scale bar indicates 1 mm for (a) and (c).

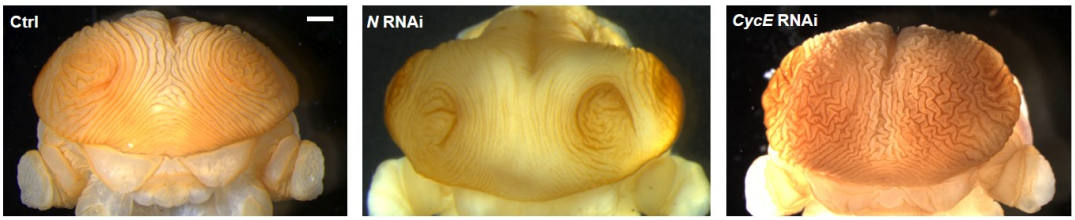


Figure 2-3-11. Comparison of 2D furrow pattern between control and *N* and *CycE* RNAi

Comparison of surface 2D furrow pattern between control and *N* and *CycE* RNAi. Two concentric-like furrows are observed in control and *N* RNAi. Zigzag pattern is observed in *CycE* RNAi.

The Notch and CyclinE genes contribute to the control of frequency and localization of mitosis, respectively

Next, in order to investigate the relationship between cell division and 2D furrow pattern and furrow depth in cap region, I analyzed the orientation, frequency and localization of cell division in the mushroom-shaped cap region (Fig. 2-3-12 a) among control, *N* RNAi and *CycE* RNAi primordia. In all the experimental groups, including the control, there was no clear anisotropy of cell division in any measured region of the primordial cap (Fig. 2-3-12 b, c, 2-3-13). Thus, region-specific anisotropy of cell division is not likely to be involved in furrow depth control and region-specific 2D furrow patterns. On the other hand, in control primordia, a specific localization pattern of mitosis was observed among the regions (Fig. 2-3-12 d). The frequency of mitosis in the right and left parts were twice as high as in the other parts (Fig. 2-3-12 d). In *N* RNAi, total mitosis was decreased in all the measured regions, while its distribution pattern was not changed (Fig. 2-3-12 d). In *CycE* RNAi, the specific localization pattern of cell division was disturbed. That is, the frequency of mitosis in the right and left parts of the primordium was decreased, which resulted in a uniform distribution of mitosis across the regions (Fig. 2-3-12 d).

A number of studies have reported that Notch contributes to cell proliferation in insect development (i.e. labrum of Tribolium castaneum, the eye and the wing of Drosophila melanogaster)(Baonza and Garcia-Bellido 2000, Kenyon et al. 2003, Siemanowski et al. 2015). Hence, in beetle horn development, Notch is also assumed to contribute to cell proliferation. However, the relationship between the frequency of mitosis and the depth of the primordial furrow is still unknown. Notch signaling is also well known to contribute to joint formation in insects (de Celis et al. 1998). The mechanism of furrow formation may be similar to joint formation because both of them include the folding of epithelial cell sheets (Cordoba and Estella 2018). In the future, research about joint formation may provide avenues to further understand furrow formation.

As can be seen from nuclei staining images, the fluorescence intensity of Hoechst was higher in specific areas of control and *N* RNAi horn primordia (Fig. 2-3-12 a, yellow circle), but this fluorescence pattern was not detected in *CycE* RNAi. This means these brighter areas contained more cells in the S/G2 phase of the cell cycle because the fluorescence intensity of Hoechst is dependent on ploidy. The *CycE* gene is involved in the progression of the cell cycle, especially the transition from G1 to S phase (Edgar and Lehner 1996). Hence, it assumed that *CycE* RNAi decreased mitosis in a specific area. The region where the frequency of cell division was disturbed in *CycE* RNAi and the region where the 2D furrow pattern (concentric-like pattern) was disturbed in *CycE* RNAi were identical, suggesting that the cell division distribution pattern can affect the 2D furrow pattern. Although the developmental link between the cell division distribution and final 2D furrow pattern is still unknown, one of the possibilities is that specific mechanical stress caused by differences of cell division frequency may determine the direction of furrows.

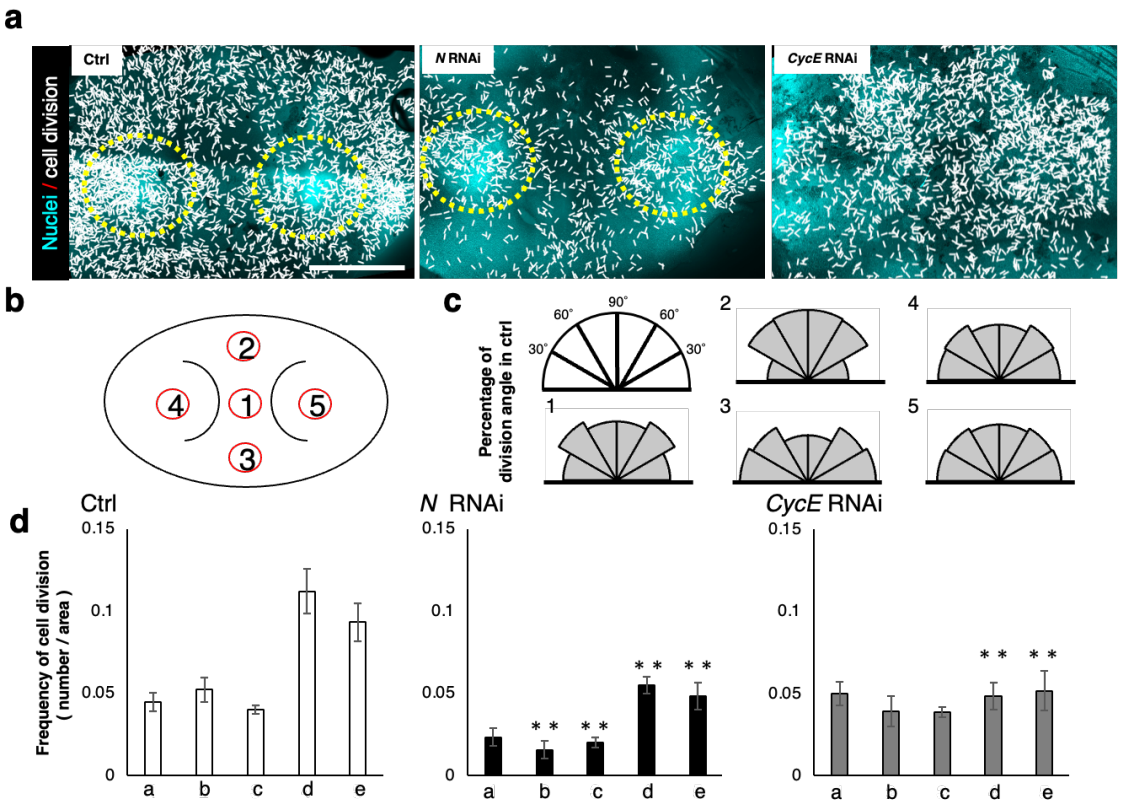


Figure 2-3-12. Analysis of cell division of the primordia

(a) Plot of the orientation and the localization of cell division in control and *N* RNAi and *CycE* RNAi. Each white line indicates one dividing cell. Direction of white line shows the orientation of cell division at that point. Yellow circles show the area of high intensity of Hoechst fluorescence. (b) The area of measured cell division. Five regions were determined by using a pair of characteristic crescent shape furrows as landmarks. This furrow stably formed as the first furrow in all the analyzed primordia. (c) Plot of the percentage of the orientation of cell division in five areas of the primordia. Significant change of cell division orientation was not detected (n = 5, for negative control). The results for RNAi are shown in Figure 2-3-13. (d) Quantification of frequency of cell division in five areas of the primordia. In control and *N* RNAi, the frequency of mitosis in the right and left parts were twice as high as in the other parts. *N* RNAi decreased the number of cell divisions in all areas of the primordia. *CycE* RNAi decreased cell division only in both side areas of the primordia. Double asterisk (**) indicates the statistical significance comparing the same area of

primordia between *N* or *CycE* RNAi and negative controls (n = 5, 4, 5 for negative control, *N* RNAi, *CycE* RNAi, respectively). Scale bar indicates 1 mm for (a).

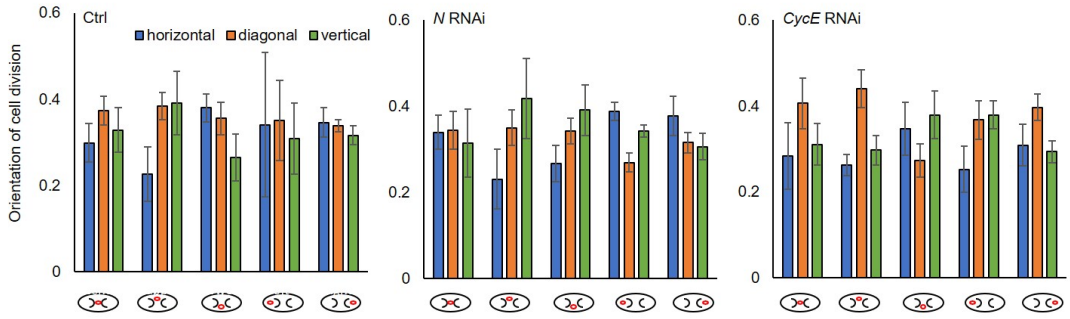


Figure 2-3-13. Comparison of cell division angle between control and *N* and *CycE* RNAi

Blue bar shows the ratio of cells divided in horizontal direction ($0 < \theta \leq 30$). Orange bar shows the ratio of cells divided in diagonal direction ($30 < \theta \leq 60$). Green bar shows the ratio of cells divided in vertical direction ($60 < \theta \leq 90$). None of the RNAi treatments showed significant change of cell division orientation for any area.

## 2.4 Conclusion

In this section, I revealed that morphological parameters (macro structure and micro furrow 2D pattern and depth) in the horn primordia were controlled by different mechanisms. That is, macro structure size is controlled in a body-size dependent and Dachsous dependent manner while micro furrow depth and 2D pattern are not. The depth and 2D pattern of micro furrows are controlled independently via Notch signaling and CyclinE-dependent mechanisms, respectively (Fig. 2-4-1). Any one of these morphological parameters can be changed independently, which then alters the final 3D horn shape as well.

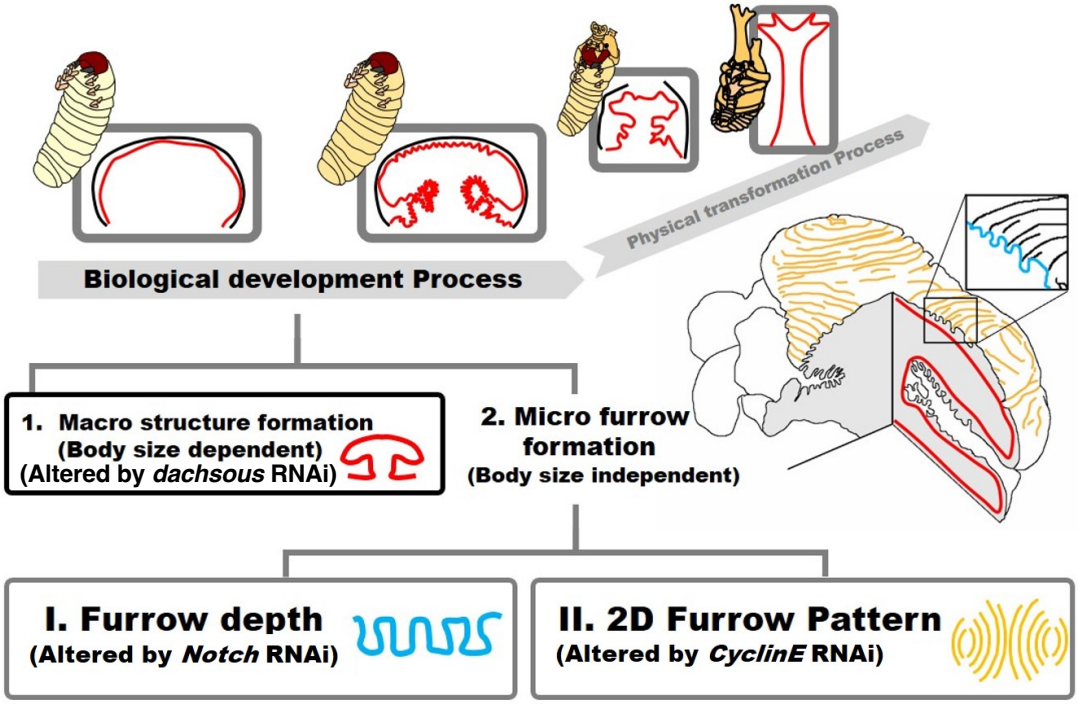


Figure 2-4-1. Summary of beetle horn development via “folding and extension”

In the “folding and extension” seen in beetle horn development, the final 3D shape has been already coded when the folding process is done. In this study, I demonstrated that the folding process can be divided into 1) macro structure formation and 2) micro furrow formation. Macro structure formation can be regulated via Dachsous control and body size dependent control. Micro furrow formation can be further divided into depth regulation and 2D pattern formation via Notch and CyclinE control, respectively.

# Chapter 3

# Development of treehopper helmet

## 3.1 Introduction

Arthropods are covered with a rigid exoskeleton that protects the body physically and chemically (Hopkins and Kramer 1992, Snodgrass 1935, Chapman 1998). However, the elasticity of the exoskeleton is limited and does not allow for continuous growth. Therefore, most species of arthropods grow by shedding their hard cuticle, a phenomenon known as molting (Snodgrass 1935, Chapman 1998, Kramer and Koga 1986). In order to develop a complex structure through molting, a new exoskeleton with a folding structure must be formed before the molt. The folding structure are then extended to form a complex three-dimensional structure through molting. In beetle horns, previous studies have demonstrated by experiment and computer simulation that the folding expansion process is a simple physical transition that does not involve cell division, migration, apoptosis, or other cellular activities (Matsuda et al. 2017). Thus, the final structure is uniquely determined at the completion of the primitive morphogenesis. Given the diversity of morphologies in arthropod exoskeletons, this "morphogenesis by folding and elongation" may be capable of forming a variety of final 3D shapes. However, the developmental process by which these primordia have specific grooves and encode various three-dimensional structures has hardly been elucidated except for the horn of the beetle and few model insects, which was analyzed in Chapter 2.

The most extreme example of a three-dimensional structure formed by molting is the helmet (enlarged pronotum) of the treehopper (Insecta: *Hemiptera*: *Auchenorrhyncha*: *Membracidae*) (Fig. 1a-f). The three-dimensional shape of the treehopper helmet is extremely diverse, including branched TV antennae (e.g., *Bocydium* Fig. 3-1-1 a), roofs (e.g., *Adippe* Fig. 1b), crescents and more complex C shapes (e.g., *Cladonota* Fig. 3-1-1 c-d), elongated cylinders (e.g., *Polyglypta* Fig.3-1-1 e), spiky to forked (e.g. *Poppea* Fig. 3-1-1 f), or ant-like shapes (Wood 1993, Godoy-Cabrera et al. 2006, Cryan et al. 2004). These complex 3D shapes appear during the molt from the last instar nymph to the adult (Stegmann 1998, Prud'homme et al. 2011). During the molt, both the size and the shape of the

helmet change significantly over a short period of time. Given the metamorphosis that leads to the short time emergence of the adult helmet, it is likely that the helmet primordium beneath the cuticle of the final nymph has already formed a specific folding and furrow pattern on the epithelial and cuticle sheet.

There are two structural transitions in the emergence of the adult helmet. The first is the transition from a single-layered sheathing pronotum to a two-layered plywood helmet. Morphological studies have shown that the adult helmet is plywood-like and two-layered, whereas the larval pronotum is sheath-like and one-layered (Stegmann 1998).

The second is the size transition from a small helmet to a large helmet. It would be very interesting to know when and in what order these two changes take place in the larval cuticle.

Few studies on the morphogenesis of the treehopper helmet have been reported, except for a few molecular studies focusing on wing development genes (Prud'homme et al. 2011) and transcriptome profiles (Fisher, Wegrzyn and Jockusch 2020), and especially few histological and anatomical descriptions. In this study, using micro-CT, scanning electron microscopy (SEM), and paraffin sections of *Antianthe expansa* (Germar, 1835) (*Smiliinae: Smiliini*), a species of roofed-helmeted trematode, to investigate two structural transitions were revealed, showing the developmental trajectory and structure of the helmet. *Antianthe expansa* was chosen for the first analysis of many treehoppers because the larvae and adults congregate in groups in one place (Fig. 3-3-1 A), making it easy to obtain a large number of samples.

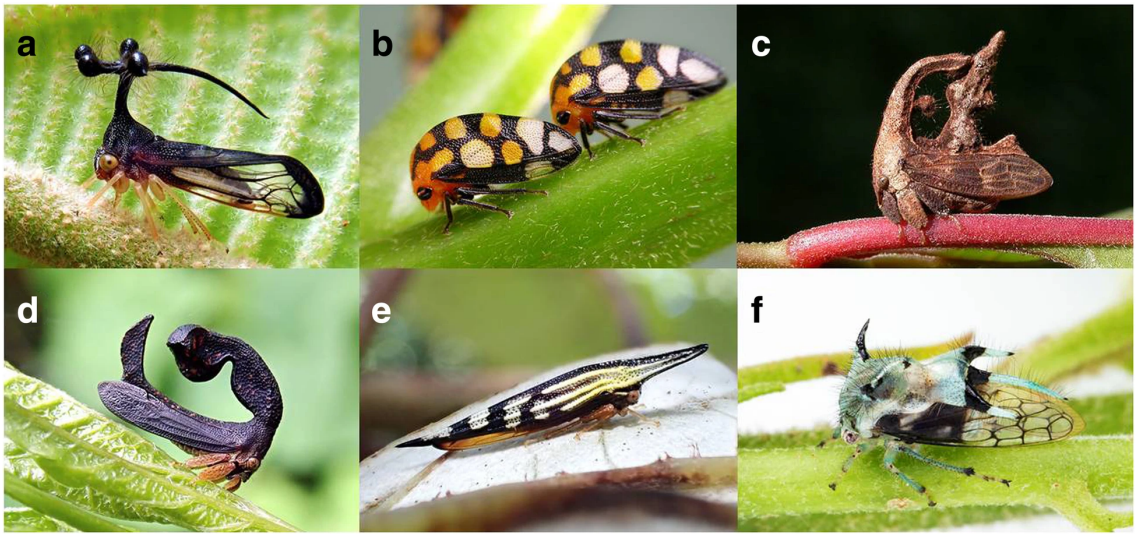


Figure 3-1-1. Various 3D morphologies of treehopper helmets.

The morphology and color of treehopper helmets show a wide diversity. All species shown here occur in Costa Rica: a *Bocydium mae*. b *Addipe zebrina*, c *Cladonota biclavata*, d *Cladonota sp.*, e *Polyglypta sp*., f *Poppea sp*

## 3.2 Material and method

Insect Collecting

Treehopper samples, nymphs and adults were collected at the Universidad de Costa Rica, San Pedro de Montes de Oca, San José, Costa Rica in November of 2016 2017 and 2019. Sampled insects were immediately fixed in formalin and 95% EtOH. Movies of the imaginal molt were recorded with a hand digital video camera (iVIS, Canon, Japan), by bringing late-stage final instar nymphs back to a hotel room. All collecting was done correctly with the permission of MINAET-SINAC, Costa Rica, resolution numbers SINAC-SE-GASP-PI-R-122-2016, 056-2017-ACC-PI, M-P-SINAC-PNI-ACAT-047-2017.

Micro-CT scanning

In order to observe the adult helmet and developing nymphal helmet structure, I scanned treehoppers by using a micro–CT-scanner SkyScan 1172 (SkyScan NV, Belgium) following the manufacturer's instructions. Sample preparation was performed as follows. Formalin fixed samples were dehydrated with 50/75/90/100% ethanol over 30 minutes in each step. Dehydrated samples were soaked in t-butanol and freeze-dried (FZ-2.5; Asahi Life Science, Japan). Dried samples were mounted on rubber putty to fix them during scanning. The X-ray source and resolution was 30-50 kV and 2.5 um/pixel, respectively. Suitable settings were used depending on the sample and purpose of the scan. Scanned primary shadow images were reconstructed into stacks of sections via SkyScan software NRecon (Version 1. 7. 1. 0) and then 3D volume-rendered images were constructed using SkyScan software CT Vox (Version 3. 3. 0). Movies and images of the constructed 3D volume-rendered images were also recorded by software function of CT Vox.

Paraffin sections

Paraffin sections were prepared to observe the inner morphology of the helmet. Formalin fixed samples were transferred to 70% ethanol overnight and then dehydrated with 90, 95 and 100% ethanol, and finally cleared in xylene. Cleared samples were embedded into paraffin and sectioned (6

um) with a microtome (RM2135, Leica, Germany). Sections were stained with hematoxylin and eosin, then captured with microscope (BZ-X700, Keyence, Japan).

Scanning electron microscopy (SEM)

Sample preparation was performed as follows. For observing the developing helmet inside the nymphal cuticle, I removed nymphal cuticles from formalin-fixed final instar nymphs with forceps under a binocular microscope. Dissected samples were then dehydrated with 50/75/90/100% ethanol for 30 minutes during each step. Samples were then soaked in t-butanol. The samples were dried with a freeze-dry system (FZ-2.5; Asahi Life Science, Japan) and coated with Au with DII-29010SCTR Smart Coater (JEOL Ltd., Tokyo, Japan). Prepared samples were observed with a scanning electron microscope JCM-6000plus (JEOL Ltd., Japan).

## 3.3 Result and discussion

Structure of adult helmet

The adult helmet of *Antianthe expansa* covers most of the dorsal part of the body (Godoy-Cabrera et al. 2006) (Fig. 3-3-1 A-D) and had a pair of lateral projections (humeral horns) at its anterior end (Fig. 3-3-1 E). The helmet was connected to the body only at the anterior margin (Fig. 3-3-2 C, C'), covering the mesosoma, metanotum and abdomen, with no other connections (Fig. 3-3-2 C, D). Thus, the space covered by the helmet is actually outside the body.

In the posterior half of the helmet there was a wall-like structure that bridges the left and right sides (Fig. 3-3-2 C-F). This structure is called a septum and was first named by Buckton and Poulton in 1903 (Stegmann 1998, Buckton and Poulton 1903). Detailed observations with paraffin sections showed that the helmet consists of two layers of cuticle (Fig. 3-3-2 B', B", C', C"). The space between the two layers was the interior of the body, and unstructured tissue and cells are also observed between these layers (Fig. 3-3-2 B', B", C', C"). Inside the helmet there are tubular structures, the apical area (median carina) (light blue arrows in Fig. 3-3-2 A-C) and the bottom of the helmet, beginning at the base of humeral horns and extending posteriorly (orange arrows in Fig. 3-3-2 A-C). These tubular structures are also referred to as the median and lateral ridges in a previous study (Stegmann 1998). The median ridge was connected to the body by the pronotum just behind the head, and the lateral ridges were connected by the lateral projections (Fig. 3-3-2 D). The ridge had a thicker cuticle than the rest of the body (Figs. 3-3-2 B, B') and is thought to function as the framework of the helmet. It is also expected to act as a passageway for the fluid delivered during molt to stretch the tightly folded helmet primordium. The septum also consists of two layers, both of which are connected to the lower layer of the helmet, also called the ventral lobe (Stegmann 1998) (Fig. 3-3-2 C' and C"). This means that the lower layers were folded inwards, and the folded inner layers were attached to each other to form a septum (Fig. 3-3-2 C). These structures (double-layered helmet, median carina, lateral carina and septum) have also been observed in the previously studied species *Stictocephala bisonia*, which has a roof-like helmet (Stegmann 1998). There is one difference between *Antianthe* and *Stictocephala* that the *Antianthe* has two pairs of lateral carinae (Fig. 3-3-2 B-D) while the *Stictocephala* has just one pair.

Structure of nymphal pronotum

In the last nymphal instar, the dorsal area of the pronotum extends to the posterior part of mesothorax forming a “helmet sheath” (Fig. 3-3-3 A, B). It is thought that the adult helmet, in a folded state, is stored as a primordia in the sheath just before molting. This helmet sheath was single layered, and the inner surface of the sheath was connected to the body (Fig. 3-3-3 B,C). The nymphal pronotum is a large, single-layered outgrowth of integument connecting with the body cavity (Stegmann 1998). The helmet sheath has a pair of thorn-like horns projecting laterally (Fig. 3-3-3 A, B, C arrow); however, these are absent in the adult stage. At the imaginal molt, the adult helmet formed in the helmet sheath develops and extends into a large roof-like helmet (Fig. 3-3-3 D-I). This expansion of the folding helmet is probably done by pumping blood (fluid) into the median and lateral carinae, just as blood is pumped into the veins of the wings to stretch them. This process of expansion is achieved in a short time, approximately 35 minutes. And at this stage it is expected that a low elastic cuticle layer has already been formed on the surface of the helmet. Therefore, this transition does not appear to involve cell division or other cellular activity, similar to the transition from a tightly folded horn primordium to a long branched horn in rhinoceros beetles (Matsuda et al. 2017). Thus, there were two structural transitions (1) from a single-layered sheath-like structure to a two-layered plywood-like structure, and 2) from a small helmet to a large helmet, and the preparation for these transitions was found to be already completed before the final molt. Next, to investigate how these two transitions are achieved inside the nymphal helmet sheath, the development of the helmet in the last nymph stage was analyzed.

Morphogenetic processes of helmet during nymphal stage

In order to investigate the developmental development process of the helmet, I observed the internal structure of the helmet during the development of the last instar larvae using a micro-CT scan (Fig. 3-3-4). As living treehoppers were not able to live in the laboratory due to permission restrictions, dozen final age nymphs were collected in the field and immediately fixed in place. The chronological order was reconstructed based on the development status of their wings and flight muscles. In the young final instar, before the formation of the adult helmet morphogenesis, the epithelium of the pronotum, including the helmet sheath, was a single layer, the surface of which was covered by the

nymphal cuticle. (Fig. 3-3-4 B). Morphogenesis of the adult helmet begins with apolysis of the helmet epithelium (detachment of the epithelial sheet from the old cuticle). Apolysis was most likely to occur from posterior parts (Fig. 3-3-4 C), where the lower layer was first detached from nymphal cuticle (Fig. 3-3-4 C, white arrow). Along with the apolysis process, the anterior upper layer also detached from the nymphal cuticle (Fig. 3-3-4 D, yellow arrows). At this stage, the helmet epithelium regresses like a deflated balloon, the upper and lower layers come together, and the inner space of the developing helmet appears to have almost disappeared (Fig. 3-3-4 D). This is a remarkable transition from a single layer to a double layer (Fig. 3-3-4 D). The entire newly formed helmet then contracted and the apolysis ended (Fig. 3-3-4 E). After this stage, the helmet grew larger (Fig. 3-3-4 F) and finally filled the entire space of the helmet sheath and other areas of the pronotum (Fig. 3-3-4 G). As the helmet grew, many folded structures were also formed (Fig. 3-3-4 F, G).

Next, the outer morphology and topological structure of the developed helmet (corresponding to Fig. 3-3-4 E) and the fully developed helmet (corresponding to Fig. 3-3-4 G) after contraction were then observed using scanning electron microscopy (SEM) and paraffin sections. As a result, I found that the shape of the developing helmet after shrinking was very similar to the adult helmet, although the total helmet size was still much smaller at this stage (Fig. 3-3-5 A). From the ventral side, the septum structure could also be observed (green highlighted area in Fig. 3-3-5 B). A cross-section of the helmet showed that the lower and upper layers are attached to each other, forming a two-layered structure (Fig. 3-3-5 C). The median carina and the bilayer septum are also clearly visible in this paraffin section (Fig. 3-3-5 C). Thus, at this stage, most of the characteristic components of the adult helmet structure (double layered roof shape, septum, median carina) have already appeared and this developing helmet can be called a "miniature" of the adult helmet. This means that the structural transition from a single-layered sheathing structure to a two-layered roofing structure, which is one of the two transitions mentioned above, has almost been achieved at this stage.

After this, the miniature helmet grows to its final folding structure. As it grows, a number of folding furrows are formed on the surface of the helmet. (Fig. 3-3-5 D, E, F). The size transition from the small nymphal helmet sheath to the large adult helmet sheath is probably due to growth with this furrow formation. There are at least two types of furrows. The first type consists of a deep furrow formed by the folding of a double-layered epithelial sheet (macro furrow). The most pronounced

macro furrows run along the anterior-posterior axis on both sides of the helmet (indicated by a yellow dashed line in Fig. 3-3-5 D and by arrowheads in Fig. 3-3-5 E and 3-3-5F). The second type consists of superficial dense furrows which are found on most of the helmet surface (hereafter micro furrow). Many of these micro furrows were irregularly zigzagged (highlighted in pink in Fig. 3-3-5 E) which enable the helmet to become broadened in every direction. In some specific areas, such as the surface of the median and lateral carinae, the fine furrows were arranged in regular parallel lines (highlighted in blue in Fig. 3-3-5 E), which enable the tubular structures to expand in one direction. Both macro and micro furrows might be responsible for the enlargement of the helmet and determine the rate and direction of expansion.

The cytological contribution to helmet shrinking and its re-growth with folding is still unknown, but the results suggest that various cell activities (proliferation, shape change, migration and cell death) are involved in those processes. In particular, extensive cell proliferation is likely to be involved in the growth of the miniature helmet.

In conclusion, helmet development in *Antianthe expansa* takes place as follows. The sheath-like monolayer epithelial sheet undergoes apolysis and the lower and upper layers shrink together into a miniature helmet (structural change from monolayer to bilayer). The miniature helmet then grows in size, forming both of macro and micro furrows (size transition from small to large) (Fig. 3-3-4 H).

Developmental similarities of helmet and wing

Thus, treehoppers develop a densely folded primordium prior to molt, which is then extended during molt to form a complex three-dimensional structure. This pattern of development is also seen in the development of the horns of the rhinoceros beetles (Matsuda et al. 2017) (Fig. 3-3-6). However, there is a crucial difference between the treehopper helmet and the beetle horn. In the beetle horn, the primordium is a single-layered, pouch-like structure that is elongated by the fluid pressure filling the inside of the pouch (Fig. 3-3-6). On the other hand, the treehopper helmet is made of a double layered, plywood-like structure, which is extended through a tubular carina by the pressure of bodily fluids (Fig. 3-3-6).

The treehopper helmet shows similarities to the development of wings in the change from a single to a double layered structure (Fig. 3-3-6). In hemipterous insects, the wing develops as a single-layered structure within a sac-like wing bud, which changes during development into a two-layered planar two-dimensional structure (Snodgrass 1935) (Fig. 3-3-6). Initially, the bilayer wing was a small miniature of the adult wing (Fig. 3-3-6), but subsequent cell proliferation allowed the bilayer sheet to bend to form dense furrows that allowed the wing to grow (Fig. 3-3-6). Even in the highly derived Drosophila wing development, the dorsal and ventral epithelia come together during development to form a two-layered, flattened miniature wing (Waddington 1940). In addition, the furrows are extended by pumping hemolymph through tubular structures on both the helmet (carina) and wing (vein). (Fig. 3-3-6). Although the anatomical homology between the helmet and wing is not supported (Mikó et al. 2012, Yoshizawa 2012), recent molecular developmental studies suggest that the wing and helmet share the same molecular networks. That is, genes important for wing development are expressed in the developing helmet (Prud'homme et al. 2011) and the transcriptome profile of the developing helmet shows more similarity to the developing wing than to other body parts (e.g. legs and arthropods) (Fisher et al. 2020). The similarities in the development of helmets and wings shown in this study also support this idea.

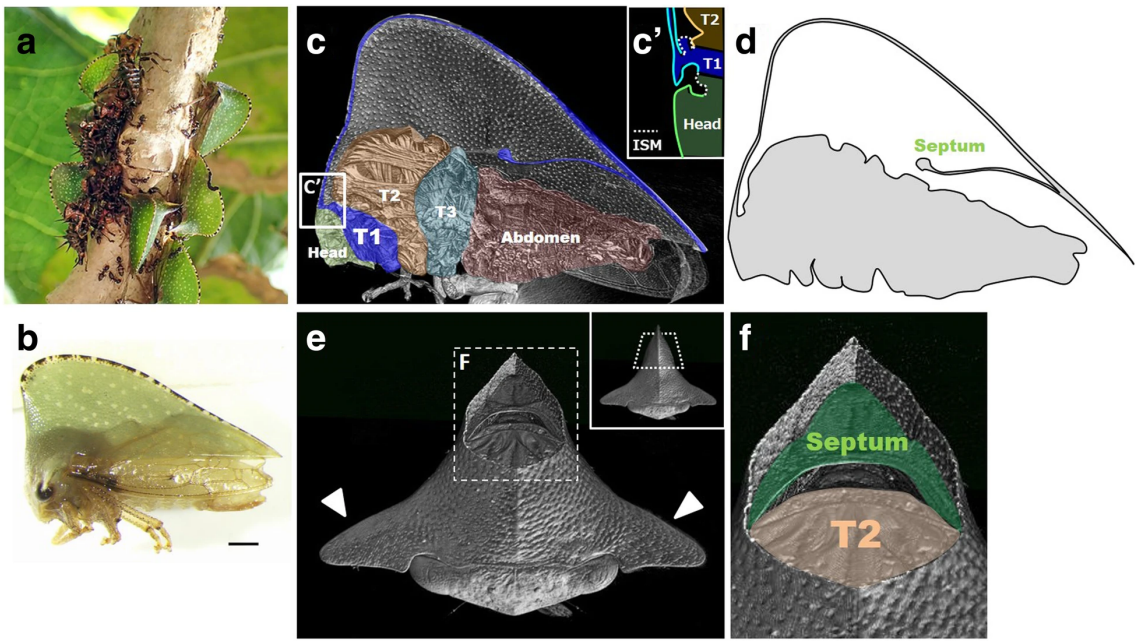


Figure 3-3-1. Adult morphology of focal species, Antianthe expansa.

(a) Adults and nymphs of Antianthe expansa in the field. Adults and various nymphal instars are present on the same branch and are often associated with ants. (b) Side view of adult. Scale bar indicates 1 mm. (c) Virtual sagittal section of adult via micro-CT scan imaging. Head, prothorax (T1), mesothorax (T2), metathorax (T3) and abdomen are indicated in different colors. Connection point of head, helmet (dorsal prothorax), and mesothorax is magnified in C'. ISM: intersegmental membrane. (d) Diagram of cross section of C. It can be clearly seen that the helmet is a thin structure and connects only at the most anterior region. (e) Frontal view of adult via micro-CT imaging. The dorsalmost region of the helmet was graphically excised to show the inner side of the helmet. White arrows indicate a pair of lateral projections (humeral horns). (f) Magnified image of dashed window in E. Highlighted in green is the septum and in orange is dorsal part of the mesothorax (T2)

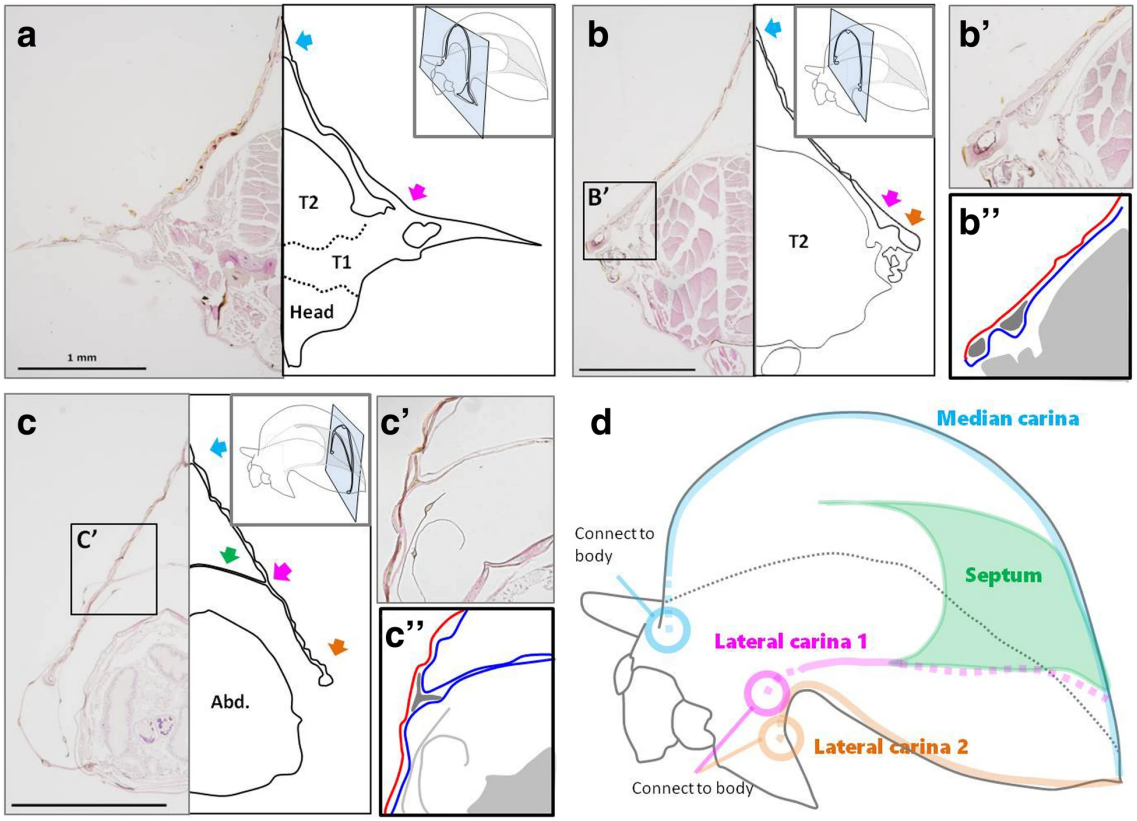


Figure 3-3-2. Structure of adult helmet of Antianthe expansa.

(a-c) Frontal section of adult Antianthe expansa. (a) Frontal section at lateral projection. A connection between lateral carina 1 (pink arrow) and the body is clearly recognizable. There is a tubular structure at the top of the helmet known as the median carina (blue arrow). (b) Frontal section at middle mesothorax. Note that the helmet and body are not connected. There are two tubulars lateral carinae on each side of the helmet (pink and orange arrow). B′) Magnified image of lateral carinae which have a thicker cuticle. Also, it can be clearly seen that the helmet is double layered. B″) Schematic drawing of B′. Red and blue line indicate upper and lower layer, respectively. Dark gray indicates inner space of lateral carinae. c Frontal section at abdomen. The septum (green arrow) bridges both sides of the helmet. C′) Magnified image of connected area of septum. The septum is composed of two thin layers of cuticle, so that the septum is also double layered. C″) Schematic drawing of C. Red and blue line indicate upper and lower layer, respectively. Both of the two layers comprising the septum are from the lower layer. d Schematic summary of adult helmet structure

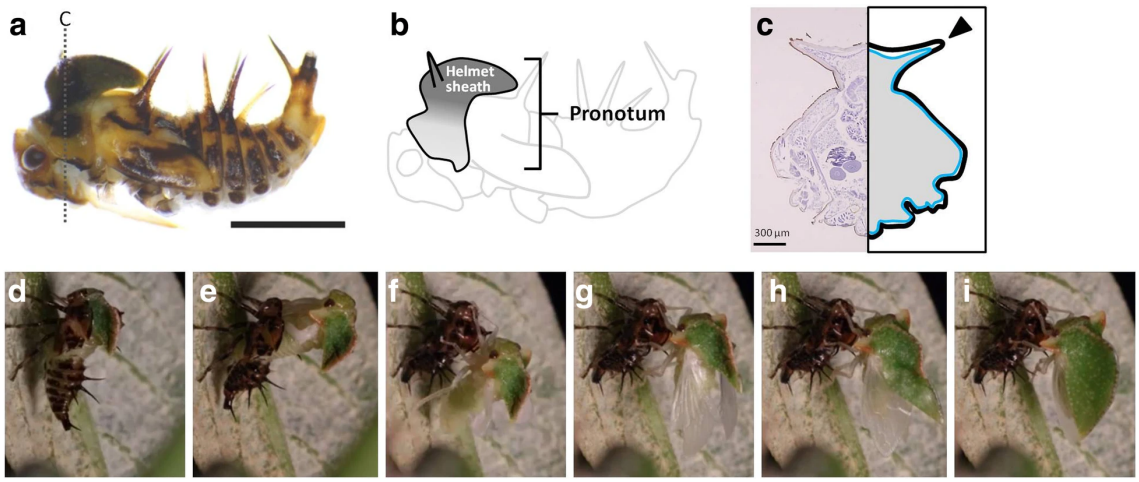


Figure 3-3-3. Structure of nymphal pronotum of Antianthe expansa.

(a) Side view of last instar nymph of Antianthe expansa (legs were removed). Scale bar indicates 2 mm. Sectioned region in (c) is indicated as a dashed line. (b) Schematic summary of pronotum and helmet sheath of final instar nymph. The dorsal projected region of the nymphal pronotum was called a “helmet sheath” indicated in dark gray. There is no clear border between the helmet sheath and other parts of the pronotum. (c) Frontal section of nymph. Note that the helmet sheath is monolayer (the epithelium is indicated by a blue line) and the inside of the helmet sheath is filled with tissue. d-i Time-lapse images of eclosion of an adult Antianthe expansa. Extremely folded structures (dense furrows) were extended to form the final 3D helmet structure. This transformation occurs in approximately 35 min, which indicates that cytological activities (e.g., cell division and migration, etc.) cannot play important roles in this extension

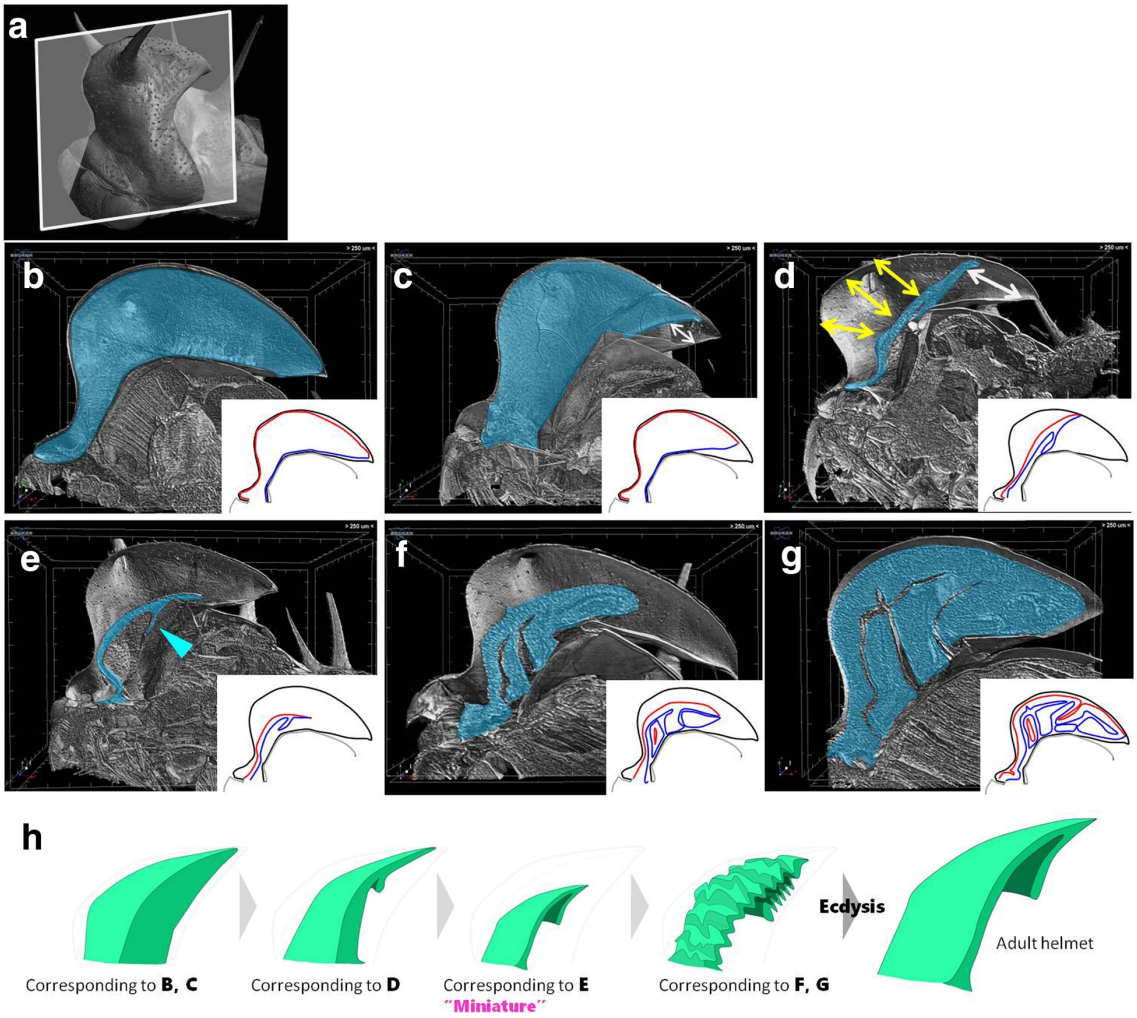


Figure 3-3-4. Helmet morphogenesis inside the nymphal helmet sheath in Antianthe expansa.

(a) Surface view of last instar nymph of Antianthe expansa via micro-CT scan. White window indicates sectioned region in B to G. (b-g) Sagittal section of last instar nymph. The developing adult helmet primordium is highlighted in blue. Schematic diagrams of developing helmet are shown in small windows in each panel. Black lines, red lines and blue lines indicate nymphal cuticle, upper layer and lower layer, respectively. (b) At an early stage of the last instar nymph (before apolysis), the helmet was a monolayer, sac-like structure. (c) Once apolysis started, the helmet epithelium detached from the nymphal cuticle. First, the lower layer of most posterior region detached, indicated by a white arrow. (d) Both upper and lower layer detached from the nymphal cuticle (yellow arrows and white arrow) and came together to form a thin, double-layered plate-like structure. (e) Shrunken miniature of adult helmet has formed. At this stage a bi-layer septum also formed (blue arrowhead). (f) Miniature grows, probably by cell proliferation. During this stage both macro and micro furrows

are developed. (g) Fully developed helmet primordium which fills the entire space of the helmet sheath. The bi-layer epithelial sheet is highly complex in three dimensions, so that it is difficult to understand its structure from a single section. (h) Schematic diagram of helmet development during the last instar nymph

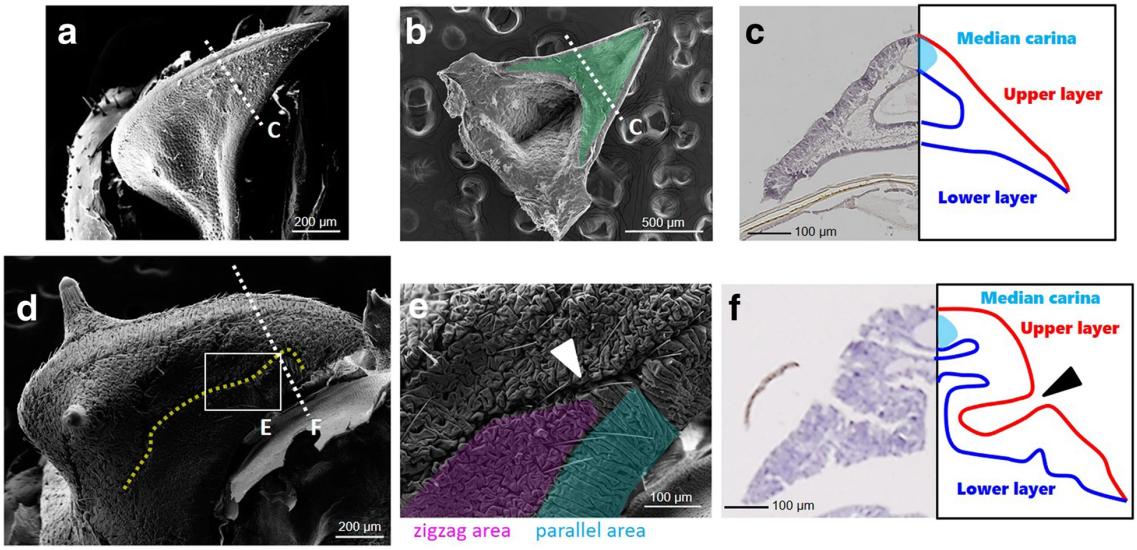


Figure 3-3-5. Observation of developing helmet via SEM and paraffin section.

(a) Whole morphology of developing miniature helmet by scanning electronic microscope (SEM) after removing outer nymphal cuticles. (b) Ventral view of miniature helmet by SEM. Septum is highlighted in green. (c) Paraffin section of miniature helmet. Upper (red line) and lower (blue line) layers can be recognized. Also, the median carina has already formed at top of the helmet, indicated as light blue. (d) Whole morphology of fully developed helmet by SEM after removing outer nymphal cuticles. (e) Magnified view of surface of the helmet. There are dense micro furrows and deep macro furrows (white arrowhead). Some areas have zigzag micro furrows (highlighted in pink) and some have parallel regular furrows (highlighted in blue). The micro furrows determine the rate and direction of expansion when extended. (f) Paraffin section of fully developed folded helmet. A deep macro furrow was made by bending the bi-layer cell sheet (black arrowhead)

## 3.4 Conclusion

In this study, the morphogenesis process of the complex 3-D morphology of the treehopper helmet was observed. The observed developmental patterns suggest that the 3D helmet morphology of the treehopper consists of 1) the formation of a miniature helmet with structures characteristic of adult helmets (e.g., a two-layered structure with septa), 2) the miniature helmet grows while forming macro and micro furrows, and finally 3) the furrows are extended during molting to form the 3D helmet morphology. Future studies should investigate the mechanisms that create the miniature helmet and the formation of region-specific grooves to better understand the most spectacular 3D morphologies found in nature.

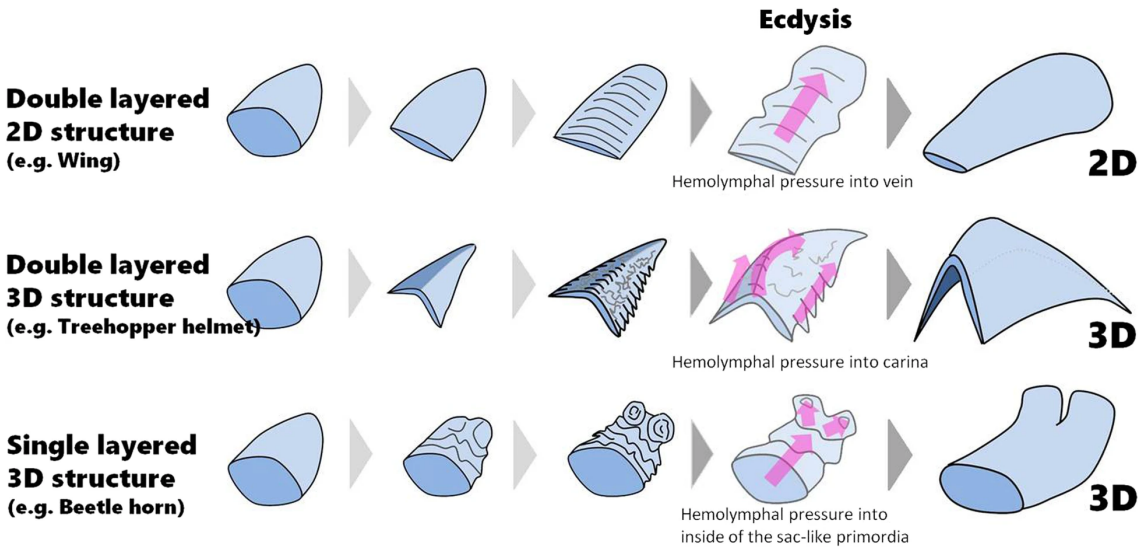


Figure 2-4-1. Schematic diagram of 2D and 3D morphogenesis of insect adult structures via "folding and extension".

All structures essentially started from a sac-like monolayer structure, but the final structures differ (2D or 3D, monolayer or double layered). In a bi-layer 2D structure like an insect wing, internal space disappears during development by connecting the upper and lower layers. Then, flat bi-layer primordia form relatively simple parallel furrows which enable primordia to enlarge in a single direction. In a bi-layer 3D structure like the treehopper helmet, upper and lower layers stick together to form a bi-layer sheet. In contrast to the wing, this bi-layer structure has a 3D shape. The macro and micro furrows determine the expansion rate in multiple direction to form its 3D shape. In a monolayer 3D structure, the inner space of the primordium does not disappear during development. Furrows are formed in the surface of the primordium by bending a single layer of epithelium and are extended by hemolymphal pressure at molting

# Chapter 4
# General conclusion and Future direction

In this study, I investigated the mechanism of morphogenesis by molting in arthropods. In Chapter 2, I focused on the morphogenesis of the horn of the beetle. First, from the analysis of *ds* RNAi horn primordia, I showed that the structure of the horn primordium can be divided into macro shape morphogenesis and micro furrows formation on its surface. Furthermore, through RNAi screening, I identified genes that are important for the depth and concentric circle pattern of the micro furrows, indicating that the micro furrows can be further divided into the depth and the pattern. I also found cytological phenomena (anisotropy of cell division, localization pattern of cell division, and number) that are thought to be important for each structure. In Chapter 3, I focused on the morphogenesis of the helmet of the treehopper, which has a great variety of shapes among closely related species. By histological analysis of the helmet structures of adults and larvae of various stages of the species *Antianthe*, I found that even in the treehopper helmet, there is a stepwise process of macro shape morphogenesis and micro furrows formation. Namely, it was found that the epithelial cell sheet in the larval cuticle once shrank significantly to form a miniature version of the adult, and then expanded to form numerous furrows, revealing a formation process common to insects with complete and incomplete metamorphosis.

On the other hand, there are still many points of morphogenesis by molting that are not well understood. Particularly of interest are the principles that form and orientate the folding. Current observations of fixed samples in beetle horn primordia confirmed that an accumulation of F-actin is present before the cell sheet is folded, which suggests the possibility that active cellular behaviors, due to apical constriction, is a factor in the formation of furrows (Fig. 4-1). On the other hand, computer simulation and analogue simulations using cloth have shown that buckling can also produce furrows similar to those seen in beetle horns (Matsuda et al. 2021, Inoue, Tateo and Adachi 2019). In order to understand the underlying principles that give rise to cell sheet folding, it is important to observe live cell behaviors as the folding occurs. Due to various factors such as the size and transparency of the two tissues mentioned above, it is difficult to observe live the process of

their morphogenesis. Therefore, it requires other tissues suitable for in vivo live observation. In insect model animal *Drosophila*, the very dense and evenly spaced folds seen in beetles and treehoppers have not been observed (Fig. 4-2) (Domínguez-Giménez, Brown and Martín-Bermudo 2007). Crustaceans, like insects, are covered with a cuticle (Havemann et al. 2008), and many species have transparent tissue. It is therefore highly likely that crustaceans, like insects, have a folded primordium. In fact, the observation of a molting shrimp (*Neocaridina denticulate*) showed a dense, evenly spaced, directional folding (Fig. 4-2). Using the crustacean *Parhyale hawaiensis*, it has been possible to analyze the phenomenon of leg regeneration at the cellular level in a live imaging (Alwes, Enjolras and Averof 2016). In the future, the use of *Parhyale* and *Neocaridina* will help to elucidate the detailed mechanism of morphogenesis via folded primordia in arthropods.

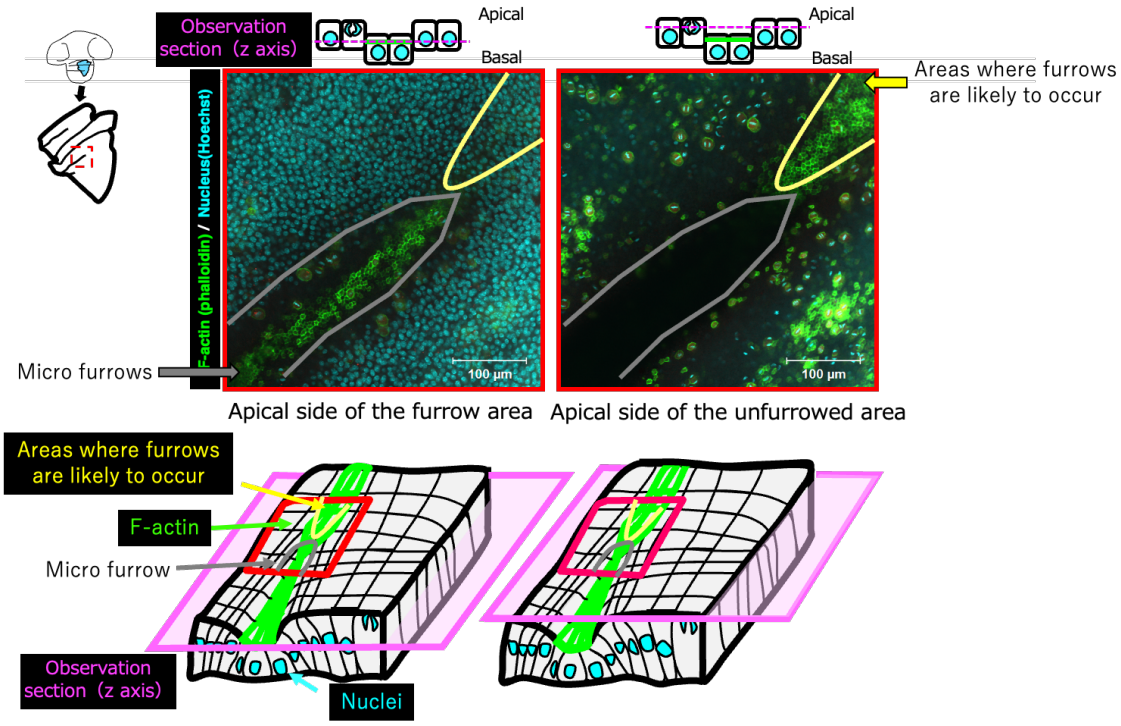


Figure 4-1. Schematic diagram of F actin accumulation in beetle horn primordia.

An accumulation of F-actin occurred at the site of the micro furrow and at the site where it will be micro furrow.

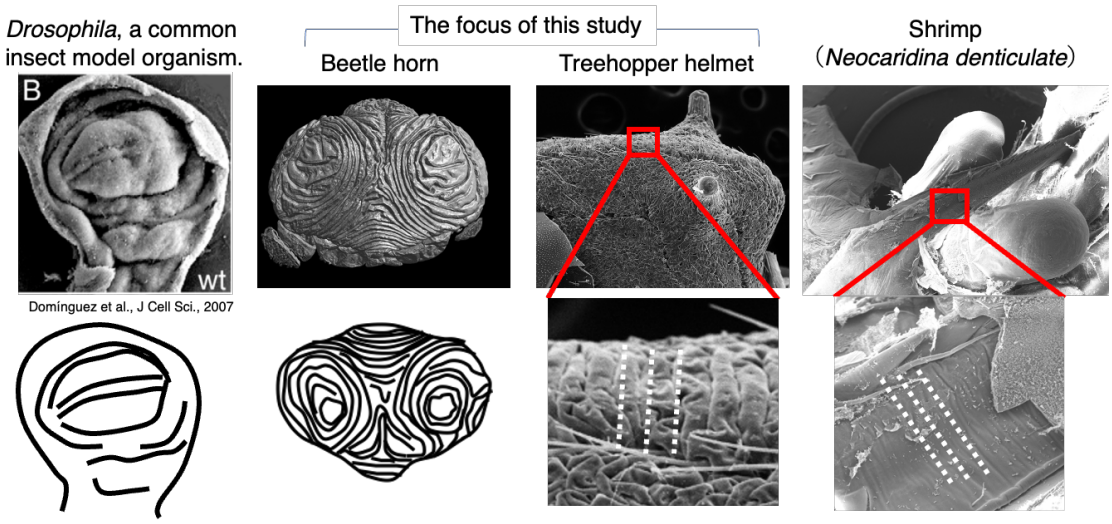


Figure 4-2. Difference of the primordial folding among species.

The dense, evenly spaced, directional folding observed in beetles and treehoppers was not observed in the insect model organism *Drosophila*, but in the rostrum in crustacean shrimp *Neocaridina*.

# Reference


Aldaz, S., L. M. Escudero & M. Freeman (2010) Live imaging of Drosophila imaginal disc development. *Proceedings of the National Academy of Sciences,* 107, 14217-14222.

Alwes, F., C. Enjolras & M. Averof (2016) Live imaging reveals the progenitors and cell dynamics of limb regeneration. *Elife,* 5.

Angelini, D. R., F. W. Smith & E. L. Jockusch (2012) Extent With Modification: Leg Patterning in the Beetle Tribolium castaneum and the Evolution of Serial Homologs. *G3-Genes Genomes Genetics,* 2, 235-248.

Baena-López, L. A., A. Baonza & A. García-Bellido (2005) The orientation of cell divisions determines the shape of Drosophila organs. *Current Biology,* 15, 1640-1644.

Baonza, A. & A. Garcia-Bellido (2000) Notch signaling directly controls cell proliferation in the Drosophila wing disc. *Proceedings of the National Academy of Sciences of the United States of America,* 97, 2609-2614.

Buckton, G. B. & E. B. Poulton. 1903. *A Monograph of the Membracidae*. L. Reeve & Company, limited.

Callaini, G., M. G. Riparbelli, M. Cintorino, S. a. Tripodi, G. Bianciardi, P. Tosi & R. Dallai (1994) The proliferating cell marker monoclonal antibody Ki-67 recognizes specific antigens associated with the nuclear envelope of the early Drosophila embryo. *Biology of the cell / under the auspices of the European Cell Biology Organization,* 81, 39-45.

Carroll, J. E. (1989) Growing Button Mushrooms.

Chapman, R. F. 1998. *The insects: structure and function.* . Cambridge university press.

Cordoba, S. & C. Estella (2018) The transcription factor Dysfusion promotes fold and joint morphogenesis through regulation of Rho1. *Plos Genetics,* 14.

Crabtree, J. R., A. L. M. Macagno, A. P. Moczek, P. T. Rohner & Y. Hu (2020) Notch signaling patterns head horn shape in the bull-headed dung beetle Onthophagus taurus. *Development Genes and Evolution*.

Cryan, J. R., B. M. Wiegmann, L. L. Deitz, C. H. Dietrich & M. F. Whiting (2004) Treehopper trees: phylogeny of Membracidae (Hemiptera: Cicadomorpha: Membracoidea) based

on molecules and morphology. *Systematic Entomology,* 29, 441-454.

de Celis, J. F., D. M. Tyler, J. de Celis & S. J. Bray (1998) Notch signalling mediates segmentation of the Drosophila leg. *Development,* 125, 4617-4626.

Domínguez-Giménez, P., N. H. Brown & M. a. D. Martín-Bermudo (2007) Integrin-ECM interactions regulate the changes in cell shape driving the morphogenesis of the Drosophila wing epithelium. *Journal of Cell Science,* 120, 1061-1071.

Edgar, B. A. & C. F. Lehner (1996) Developmental control of cell cycle regulators: A fly's perspective. *Science,* 274, 1646-1652.

Emlen, D. J., L. Corley Lavine & B. Ewen-Campen (2007) On the origin and evolutionary diversification of beetle horns. *Proceedings of the National Academy of Sciences,* 104, 8661-8668.

Emlen, D. J. & H. F. Nijhout (1999) Hormonal control of male horn length dimorphism in the dung beetle Onthophagus taurus (Coleoptera : Scarabaeidae). *Journal of Insect Physiology,* 45, 45-53.

Emlen, D. J., I. A. Warren, A. Johns, I. Dworkin & L. C. Lavine (2012) A Mechanism of Extreme Growth and Reliable Signaling in Sexually Selected Ornaments and Weapons. *Science,* 337, 860-864.

Fisher, C. R., J. L. Wegrzyn & E. L. Jockusch (2020) Co-option of wing-patterning genes underlies the evolution of the treehopper helmet. *Nature ecology & evolution,* 4, 250-260.

Fristrom, D. & J. W. Fristrom (1975) The mechanism of evagination of imaginal discs of Drosophila melanogaster: I. General considerations. *Developmental biology,* 43, 1-23.

Godoy-Cabrera, C., X. Miranda-Garnier, K. Nishida & C. Feeny (2006) Membrácidos de la América tropical= Treehoppers of tropical America.(ISBN 9968-927-10-4.).

Gotoh, H., J. A. Hust, T. Miura, T. Niimi, D. J. Emlen & L. C. Lavine (2015) The Fat/Hippo signaling pathway links within-disc morphogen patterning to whole-animal signals during phenotypically plastic growth in insects. *Developmental Dynamics,* 244, 1039-1045.

Gullan, P. J. & P. S. Cranston. 2014. *The insects: an outline of entomology*. John Wiley & Sons.

Hadley, N. F. (1982) Cuticle ultrastructure with respect to the lipid waterproofing barrier.

*Journal of Experimental Zoology,* 222, 239-248.

Hales, K. G., C. A. Korey, A. M. Larracuente & D. M. Roberts (2015) Genetics on the fly: a primer on the Drosophila model system. *Genetics,* 201, 815-842.

Havemann, J., U. Müller, J. Berger, H. Schwarz, M. Gerberding & B. Moussian (2008) Cuticle differentiation in the embryo of the amphipod crustacean Parhyale hawaiensis. *Cell and tissue research,* 332, 359-370.

Hopkins, T. L. & K. J. Kramer (1992) Insect cuticle sclerotization. *Annual review of entomology,* 37, 273-302.

Hust, J., M. D. Lavine, A. M. Worthington, R. Zinna, H. Gotoh, T. Niimi & L. Lavine (2018) The Fat-Dachsous signaling pathway regulates growth of horns in Trypoxylus dichotomus, but does not affect horn allometry. *J Insect Physiol,* 105, 85-94.

Inoue, Y., I. Tateo & T. Adachi (2019) Epithelial tissue folding pattern in confined geometry. *Biomechanics and modeling in mechanobiology*, 1-8.

Irvine, K. D. & K. F. Harvey (2015) Control of organ growth by patterning and hippo signaling in Drosophila. *Cold Spring Harbor perspectives in biology,* 7, a019224.

Ito, Y., A. Harigai, M. Nakata, T. Hosoya, K. Araya, Y. Oba, A. Ito, T. Ohde, T. Yaginuma & T. Niimi (2013) The role of doublesex in the evolution of exaggerated horns in the Japanese rhinoceros beetle. *EMBO Reports,* 14, 561-567.

Johns, A., H. Gotoh, E. L. McCullough, D. J. Emlen & L. C. Lavine (2014) Heightened Condition-Dependent Growth of Sexually Selected Weaponsin the Rhinoceros Beetle, Trypoxylus dichotomus (Coleoptera: Scarabaeidae). *Integrative and Comparative Biology,* 54, 614-621.

Kenyon, K. L., S. S. Ranade, J. Curtiss, M. Mlodzik & F. Pignoni (2003) Coordinating proliferation and tissue specification to promote regional identity in the Drosophila head. *Developmental Cell,* 5, 403-414.

Mao, Y., A. L. Tournier, P. A. Bates, J. E. Gale, N. Tapon & B. J. Thompson (2011) Planar polarization of the atypical myosin Dachs orients cell divisions in Drosophila. *Genes and Development,* 25, 131-136.

Matsuda, K., H. Gotoh, H. Adachi, Y. Inoue & S. Kondo (2021) Computational analyses decipher the primordial folding coding the 3D structure of the beetle horn. *Scientific*

*reports,* 11, 1-12.

Matsuda, K., H. Gotoh, Y. Tajika, T. Sushida, H. Aonuma, T. Niimi, M. Akiyama, Y. Inoue & S. Kondo (2017) Complex furrows in a 2D epithelial sheet code the 3D structure of a beetle horn. *Scientific Reports,* 7.

Meyer, E. J., A. Ikmi & M. C. Gibson (2011) Interkinetic nuclear migration is a broadly conserved feature of cell division in pseudostratified epithelia. *Current Biology,* 21, 485-491.

Mikó, I., F. Friedrich, M. J. Yoder, H. M. Hines, L. L. Deitz, M. A. Bertone, K. C. Seltmann, M. S. Wallace & A. R. Deans (2012) On dorsal prothoracic appendages in treehoppers (Hemiptera: Membracidae) and the nature of morphological evidence. *PLoS ONE,* 7.

Morata, G. (2001) How Drosophila appendages develop. *Nature reviews Molecular cell biology,* 2, 89-97.

Morita, S., T. Ando, A. Maeno, T. Mizutani, M. Mase, S. Shigenobu & T. Niimi (2019) Precise staging of beetle horn formation in Trypoxylus dichotomus reveals the pleiotropic roles of doublesex depending on the spatiotemporal developmental contexts. *Plos Genetics,* 15.

Ohde, T., S. Morita, S. Shigenobu, J. Morita, T. Mizutani, H. Gotoh, R. A. Zinna, M. Nakata, Y. Ito, K. Wada, Y. Kitano, K. Yuzaki, K. Toga, M. Mase, K. Kadota, J. Rushe, L. C. Lavine, D. J. Emlen & T. Niimi (2018) Rhinoceros beetle horn development reveals deep parallels with dung beetles. *Plos Genetics,* 14.

Porto, D. S., G. A. Melo & E. A. Almeida (2016) Clearing and dissecting insects for internal skeletal morphological research with particular reference to bees. *Revista Brasileira de Entomologia,* 60, 109-113.

Prud'homme, B., C. Minervino, M. Hocine, J. D. Cande, A. Aouane, H. D. Dufour, V. A. Kassner & N. Gompel (2011) Body plan innovation in treehoppers through the evolution of an extra wing-like appendage. *Nature,* 473, 83-86.

Raabe, D., P. Romano, C. Sachs, A. Al-Sawalmih, H.-G. Brokmeier, S.-B. Yi, G. Servos & H. Hartwig (2005) Discovery of a honeycomb structure in the twisted plywood patterns of fibrous biological nanocomposite tissue. *Journal of Crystal Growth,* 283, 1-7.

Ray, R. P., P. S. Ganguly, S. Alt, J. R. Davis, A. Hoppe, N. Tapon, G. Salbreux & B. J. Thompson

(2018) Apical and basal matrix remodeling control epithelial morphogenesis. *Developmental cell,* 46, 23-39. e5.

Reddy, B. V. V. G. & K. D. Irvine (2008) The Fat and Warts signaling pathways: new insights into their regulation, mechanism and conservation. *Development,* 135, 2827-2838.

Schindelin, J., I. Arganda-Carreras, E. Frise, V. Kaynig, M. Longair, T. Pietzsch, S. Preibisch, C. Rueden, S. Saalfeld, B. Schmid, J. Y. Tinevez, D. J. White, V. Hartenstein, K. Eliceiri, P. Tomancak & A. Cardona (2012) Fiji: an open-source platform for biological-image analysis. *Nature Methods,* 9, 676-682.

Segalen, M. & Y. Bellaïche. 2009. Cell division orientation and planar cell polarity pathways. In *Seminars in cell & developmental biology*, 972-977. Elsevier.

Siemanowski, J., T. Richter, V. A. Dao & G. Bucher (2015) Notch signaling induces cell proliferation in the labrum in a regulatory network different from the thoracic legs. *Developmental Biology,* 408, 164-177.

Snodgrass, R. E. 1935. *Principles of insect morphology*. Cornell University Press.

Stegmann, U. E. (1998) An exaggerated trait in insects: the prothoracic skeleton of Stictocephala bisonia (Homoptera: Membracidae). *Journal of Morphology,* 238, 157-178.

Tajika, Y., T. Murakami, K. Iijima, H. Gotoh, M. Takahashi-Ikezawa, H. Ueno, Y. Yoshimoto & H. Yorifuji (2017) A novel imaging method for correlating 2D light microscopic data and 3D volume data based on block-face imaging. *Scientific Reports,* 7.

Tomoyasu, Y. & R. E. Denell (2004) Larval RNAi in Tribolium (Coleoptera) for analyzing adult development. *Development Genes and Evolution,* 214, 575-578.

Waddington, C. H. (1940) The genetic control of wing development in Drosophila. *Journal of Genetics,* 41, 75-113.

Wang, X. F., Y. Shen, Q. Cheng, C. L. Fu, Z. Z. Zhou, S. Hirose & Q. X. Liu (2017) Apontic directly activates hedgehog and cyclin E for proper organ growth and patterning. *Scientific Reports,* 7.

Warren, I. A., J. C. Vera, A. Johns, R. Zinna, J. H. Marden, D. J. Emlen, I. Dworkin & L. C. Lavine (2014) Insights into the Development and Evolution of Exaggerated Traits Using De Novo Transcriptomes of Two Species of Horned Scarab Beetles. *Plos One,* 9.

Wood, T. K. (1993) Diversity in the new world Membracidae. *Annual review of entomology,* 38, 409-433.

Woods, D. F. & P. J. Bryant (1993) Apical junctions and cell signalling in epithelia. *Journal of Cell Science,* 1993, 171-181.

Yoshizawa, K. (2012) The treehopper's helmet is not homologous with wings (Hemiptera: Membracidae). *Systematic Entomology,* 37, 2-6.

# Acknowledgement

First of all, I would like to thank my supervisor Prof. Shigeru Kondo for his strong support of my research from various perspectives, including in terms of facilities and discussion of research direction and the results.

Also, I am deeply grateful to Dr. Hiroki Gotoh (Shizuoka University) for teaching insect experiment and discussion of research direction and the results and paraffin section analysis.

And I express my gratitude to the members of Laboratory of Pattern Formation including Dr. Keisuke Matsuda who belong to the exoskeleton group in the lab for discussion of research direction and the results.

I am grateful to Prof. Teruyuki Niimi and Dr. Shinichi Morita (National Institute for Basic Biology) and Prof. Yasuhiro Inoue (Kyoto University) for technical assistance and discussion with their unpublished data.

I also thank to Prof. Paul Hanson and Mr. Kenji Nishida (Costa Rica University) for strong technical assistance for the field work in Costa Rica and discussion and some photographs of treehoppers.

In addition, I express my thanks to Prof. Hiroshi Sasaki, Prof. Masahiro Ueda and Prof. Shin-ichi Kimura (Osaka University) for their helpful advice and for serving as the dissertation committee member of my thesis and to Prof. Toshimitsu Masuzawa (Osaka University) for helpful advice and for serving as the Human Ware Innovation Program dissertation committee member.

# Publication list

## Related Works

1) Adachi H, Matsuda K, Niimi T, Inoue Y, Kondo S, Gotoh H. (2018) Anisotropy of cell division and epithelial sheet bending via apical constriction shape the complex folding pattern of beetle horn primordia. *Mechanisms of Development*, 152: 32-37. DOI: 10.1016/j.mod.2018.06.003

2) Adachi H, Matsuda K, Nishida K, Hanson P, Kondo S, Gotoh H. (2020) Structure and development of the complex helmet of treehoppers (Insecta:Hemiptera: Membracidae). *Zoological Letters*, 6: 3. DOI: 10.1186/s40851-020-00155-7

3) Adachi H, Matsuda K, Niimi T, Kondo S, Gotoh H. (2020) Genetical control of 2D pattern and depth of the primordial furrow that prefigures 3D shape of the rhinoceros beetle horn. *Scientific Reports*, 10: 18687. DOI: 10.1038/s41598-020-75709-y

## Unrelated Work

4) Adachi H, Ozawa M, Yagi S, Seita M, Kondo S (2021) Pivot burrowing of scarab beetle (Trypoxylus dichotomus) larva. *Scientific Reports*, 11: DOI: 11.14594/s41598-021-93915-0